Pisias, N.G., Mayer, L.A., Janecek, T.R., Palmer-Julson, A., and van Andel, T.H. (Eds.), 1995
Proceedings of the Ocean Drilling Program, Scientific Results, Vol. 138

42. THE LATE MIOCENE (11–8 MA) EASTERN PACIFIC CARBONATE CRASH: EVIDENCE FOR REORGANIZATION OF DEEP-WATER CIRCULATION BY THE CLOSURE OF THE PANAMA GATEWAY[1]

Mitchell Lyle,[2] Kathleen A. Dadey,[3] and John W. Farrell[4]

ABSTRACT

In the eastern and central Pacific Ocean the most profound change in Neogene calcium carbonate deposition occurred at the late/middle Miocene boundary (about 10 Ma), when carbonate mass accumulation rates (MARs) abruptly dropped. East of the East Pacific Rise (EPR), carbonate deposition essentially ceased. The carbonate compensation depth (CCD) in the Guatemala Basin, for example, rose by 800 m in less than 0.5 Ma. Even the rise crests suffered carbonate losses—Site 846, at the time less than 300 meters deeper than the EPR axis, experienced intervals between 10 and 9 Ma where no carbonate at all was buried. By about 8 Ma carbonate deposition resumed and was concentrated along an equatorial band, suggestive of high surface water carbonate production. East of the EPR, however, CCDs remained shallow since 10 Ma. This event which we have termed the late Miocene carbonate crash marks a fundamental paleoceanographic change that occurred in the eastern Pacific Ocean.

Here, we document the changing pattern of carbonate deposition from 13 Ma to 5 Ma by using maps of carbonate MAR reconstructed from ODP Leg 138 and DSDP data. Comparisons to modern oceanographic conditions demonstrate that the late Miocene carbonate crash could not have been caused by an abrupt increase in productivity at 10 Ma or by loss of C_{org} from continental shelves. Instead it was probably caused by a relatively small reduction in deep-water exchange between the Atlantic and Pacific Oceans through the Panama Gateway prior to the emergence of the isthmus. A small restriction of deep-water exchange through this gateway is sufficient to radically change carbonate MARs in the eastern Pacific.

INTRODUCTION

The equatorial Pacific Ocean is a major sink for calcium carbonate and is an important component of the global carbon cycle. Surface sediments along the EPR and westward along the equator typically have carbonate contents greater than 80% and carbonate MARs greater than 1 g/cm^2/k.y. (van Andel et al., 1975; Lyle et al., 1988; Farrell and Prell, 1989). East of the EPR, in the Guatemala, Panama, Bauer, and Peru basins, there exists a strong depth dependence for carbonate burial (Lyle, 1992). CCDs east of the EPR are 500 to 1000 m shallower than those to the west (Berger et al., 1976). Consequently, little carbonate is buried in the deeper parts of these eastern Pacific basins, despite relatively high carbonate production by plankton (Dymond and Lyle, 1985). Here, we investigate how this distinctive regional carbonate deposition pattern has evolved.

Initial Leg 138 studies have shown that shallow CCDs first appeared in the eastern Pacific basins between 11 and 9 Ma. Simultaneously, a major carbonate MAR transient took place throughout the eastern and central Pacific Ocean (van Andel et al., 1975; Keller and Barron, 1983; Theyer et al., 1985). High carbonate MARs returned by 8 Ma, except in the easternmost Pacific. The transient has left a distinctive regional acoustic reflector in the tropical eastern and central Pacific Ocean (reflector lM-P, Mayer et al., 1986).

Several hypotheses exist to explain the cause of the late Miocene carbonate crash. It may have been caused by a high productivity event that later became confined to the easternmost Pacific (Theyer et al., 1985). Degradation of C_{org} at the seafloor produces acids that dissolve carbonate. All the carbonate in a sediment can be dissolved if the ratio of C_{org} to carbonate in falling detritus becomes high, as occurs during productivity events (Emerson and Bender, 1981; Archer, 1991). Alternatively, polar cooling may have released transient C_{org} reservoirs from continental shelves exposed by the resulting decrease in sea level (Barron, 1985). Sedimentary carbonate would be lost because the total inorganic carbon content of seawater would increase relative to its titration alkalinity, dropping $[CO_3]^{2-}$ in seawater. Compensatory dissolution of sedimentary $CaCO_3$ would maintain seawater $[CO_3]^{2-}$. Changing deposition patterns of carbonate and silica between the Atlantic and Pacific Oceans (Keller and Barron, 1983) also could have also caused the crash. The latter scenario could have been driven by disrupted mid- and deep-water circulation resulting from tectonic changes in basinal configuration or closures of oceanographic gateways. In either case, changes in carbonate depositional patterns would occur because of the global redistribution of dissolved inorganic carbon and titration alkalinity.

In this study, we use gamma-ray attenuation porosity evaluator (GRAPE), wet bulk density data, wet bulk density data from well logs, and shipboard carbonate measurements from ODP Leg 138 and DSDP drill sites to reconstruct carbonate MARs in the eastern Pacific from about 13 to 5 Ma. We contrast modern and Miocene depositional patterns and also show that the Guatemala, Panama, Bauer, and Peru basins became distinct from the tropical Pacific west of the EPR at the beginning of the late Miocene. We explore whether changes in mid-water $[CO_3]^{2-}$ content, caused primarily by the uplift of the future Isthmus of Panama, might have caused the observed MAR patterns, or whether one of the other hypothesized causes for the carbonate crash are more likely.

METHODS

Cores

We used all the drill sites from Leg 138 and the DSDP drill sites listed in Table 1. We did not use Site 504/677 (Panama Basin) in the compilation, because the site's basement age was only about 5.9 Ma and it would be of only minor importance for the carbonate maps. We also used data from surface sediments whose core locations are listed in Table 2. These data also were used to construct the maps in Lyle (1992).

[1] Pisias, N.G., Mayer, L.A., Janecek, T.R., Palmer-Julson, A., and van Andel, T.H. (Eds.), 1995. *Proc. ODP, Sci. Results,* 138: College Station TX (Ocean Drilling Program).
[2] Center for Geophysical Investigation of the Shallow Subsurface, 1910 University Drive, Boise State University, Boise, ID 83725, U.S.A.
[3] Hawaii Institute of Geophysics, University of Hawaii, 2525 Correa Rd., Honolulu, HI 96822, U.S.A.
[4] Dept. of Oceanography, 6270 University Blvd, University of British Columbia, Vancouver, B.C., Canada V6T IZ4.

Table 1. Locations of drill sites used in this study.

Drill site number	General location	Latitude	Longitude	Water depth (mbsl)	Sediment thickness (m)	Oldest sediment (Ma)
84	Panama Basin	05° **45′** N	82° **53′** W	3097	255	8.7
319	Peru (Bauer) Basin	13° **01′** S	101° **31′** W	4296	110	13.6
495	Guatemala Basin	12° **30′** N	91° **02′** W	4140	428	22.5
503	Guatemala Basin	04° **03′** N	95° **38′** W	3672	235*	7.8
572	Pacific Basin	01° **26′** N	113° **51′** W	3893	489*	15.0
844	Guatemala Basin	07° **55′** N	90° **29′** W	3415	291	17.5
845	Guatemala Basin	09° **35′** N	94° **35′** W	3704	292	16.5
846	Peru Basin	03° **06′** S	90° **49′** W	3296	422	17.5
847	Peru Basin	00° **12′** S	95° **19′** W	3334	247*	6.7
848	Pacific Basin	03° **00′** S	110° **29′** W	3856	94	11.3
849	Pacific Basin	00° **11′** N	110° **31′** W	3839	349	11.6
850	Pacific Basin	01° **17′** N	110° **31′** W	3786	400	12.0
851	Pacific Basin	02° **46′** N	110° **34′** W	3760	321	12.0
852	Pacific Basin	05° **18′** N	110° **05′** W	3860	117	10.8
853	Pacific Basin	07° **13′** N	109° **45′** W	3713	66	8.6
854	Pacific Basin	11° **13′** N	109° **35′** W	3568	46	9.6

* Sites that did not reach basement.

Shipboard Carbonate Contents

Shipboard carbonate contents reported here were analyzed by coulometric methods described in detail in the "Explanatory Notes" chapter of the *Initial Reports* volume for Leg 138 (Mayer, Pisias, Janecek, et al., 1992). Small samples of sediment (10–60 mg) were acidified to release CO_2 from the carbonates, and the quantity of CO_2 released was measured by coulometric titration in a monoethanolamine solution.

Carbonate Contents of Surface Sediments

Carbonate contents in Table 2 (eastern Pacific surface sediments) were measured in two ways. The column marked "LECO" and all organic carbon measurements were measured by the acidification/wet oxidation technique described in Weliky et al. (1983). The column marked "XRF" was calculated using a normative method from the calcium contents measured by X-ray fluorescence (XRF), assuming noncarbonate detritus has a calcium content of 0.7% (Dymond et al., 1977). Opal reported in Table 2 also was estimated by a normative technique. The techniques used in the other XRF elemental analyses are described in Finney et al. (1988). Table 2 also contains sedimentation rates that were estimated from the map shown in Lyle (1992) and bulk MARs. The MARs were constructed from the estimated sedimentation rates and by using XRF-measured chlorine contents to estimate the water content of the sediment.

Conversion of GRAPE Density and Logging Density Data to Carbonate Content

The late Miocene sediment sections in Leg 138 and DSDP drill holes typically occurred at or below the deepest intervals accessible by advanced piston coring (APC). Most Miocene sediments were recovered with extended core barrel (XCB) or rotary coring (RCB) technology. Both XCB and RCB coring result in poorer recovery than APC techniques, and piecing together complete Miocene sediment sections can be difficult. Even comprehensive carbonate analyses of all material brought back on board the drill ship can still produce a sedimentary carbonate profile that has major gaps. For this reason, we used logging data where available to estimate carbonate and generate continuous carbonate curves downhole.

Dadey and Lyle (this volume) calibrate the use of downhole geochemical measurements to generate carbonate profiles and show that geochemical logging can produce reasonable results. It is also possible, and highly desirable, to use sediment wet-bulk density measurements to produce a carbonate estimate (Mayer, 1991) because large quantities of archived density data are available from even early DSDP legs. Geochemical logs, on the other hand, have only been part of the standard logging suite for about the last 5 yr of ODP.

Derivation of Density Relationship

We improved the method of Mayer (1991) to estimate sedimentary carbonate content from density by making two simple assumptions about marine sediments and by using the definitions of sediment wet-bulk density and carbonate content. Our carbonate/wet-bulk density relationship makes matching carbonate curves less empirical than that of Mayer (1991) and more easily grasped by someone not familiar with physical properties of sediments. Our method seems to do as well as that of Mayer (1991), although we have yet to make a formal comparison between the two methods. Our estimate, like that of Mayer (1991), is based upon a "decompacted" sediment column, so that burial-induced density changes can be eliminated. Our decompaction model is slightly different from Mayer's, however, because we calibrated it with eastern Pacific sediments from Leg 138, while his was based on central Pacific data (Fig. 1). The decompaction curve we use lies between Hamilton's (1976) carbonate and diatom compaction curves. We found that the match between the calculated and observed compaction in near-equatorial sites was very good, while the match in the northernmost Leg 138 sites was not. Regional variations in compaction need to be taken into account to get the most accurate match between density and carbonate content.

To derive an equation for predicting carbonate content of the sediments from wet bulk density, we assumed these things:

1. Marine sediments in the eastern Pacific are a binary mixture of calcium carbonate and an aluminosilicate 'phase'. One can think of the aluminosilicate phase in our model as a homogeneous mixture of opal, different clays, and perhaps volcanic ash. The mixture does not change in content down the core.
2. Both carbonate and aluminosilicate phases have a characteristic water content that remains constant even when they are mixed together. The second assumption allows one to assign a specific water content to a sediment mixture and, thus, to predict carbonate from wet bulk density.

Three basic equations of sediments are also needed for the derivation, as follows:

$$\rho_{wet} = \rho_{CC} X_{CC} + \rho_{AlSi} X_{AlSi} + \rho_w X_w , \quad (1)$$

where X represents the volume fraction of each sedimentary component and r represents the density of different fractions. The subscripts *wet, CC, AlSi,* and *W* refer to wet bulk density, carbonate, aluminosilicate, and water, respectively. This equation defines the wet bulk density of the sediment in terms of the densities of the components of the sediment.

$$X_{CC} + X_{AlSi} + X_w = 1. \quad (2)$$

This equation defines the sediment volume fractions and also defines the system as closed (all phases are accounted for), and

$$CC\,\% + \frac{100\,\rho_{CC}\,X_{CC}}{\rho_{CC}\,X_{CC} + \rho_{AlSi}\,X_{AlSi}}, \quad (3)$$

where *CC%* is the carbonate content of the sediment. This equation defines carbonate percentages in terms of density relationships and volume fractions.

To simplify the equations to solve for carbonate content from wet-bulk density, we needed to use Assumption 2, that both carbonate and aluminosilicate phases have constant associated water. With this assumption, the water content can be expressed by:

$$X_w = C_{WAT}\,X_{CC} + \mathrm{AlSi}_{WAT}\,X_{AlSi}\,, \quad (4)$$

where C_{WAT} and AlSi_{WAT} are the characteristic ratios of water volume to solid volume associated with carbonate and aluminosilicate phases, respectively.

A combination of these four equations designed to eliminate all variables, except the densities of each phase and the characteristic ratios, yields the following relationship between carbonate content and wet bulk density:

$$CC\,\% = \frac{100}{1 + \left(\frac{\rho_{AlSi}}{\rho_{CC}}\left(\frac{\frac{\rho_{wet}\,(\rho_{CC} - \rho_w)}{(\rho_{wet} - \rho_w)} - (\rho_{CC} + C_{WAT}\;\rho_w)}{(\rho_{AlSi} + \mathrm{Si}_{WAT}\;\rho_w) - \frac{(\rho_{wet}\,(\rho_{AlSi} - \rho_w))}{(\rho_{wet} - \rho_w)}}\right)\right)}. \quad (5)$$

In this equation, wet bulk density is a measured quantity, the density of carbonate is 2.71 g/cm^3, and the density of water is 1.025 g/cm^3. Parameters that can be varied to fit observed carbonate contents to the theoretical relationship are the density of the aluminosilicate phase mixture (ρ_{AlSi}) and the characteristic ratios C_{WAT} and AlSi_{WAT}. Normally, however, the characteristic porosity of 100% carbonate is relatively well-defined, while that of the aluminosilicate "phase" is not. When we calibrated to measured carbonate contents we varied only the aluminosilicate parameters to get the best match to measured values.

Outline of Procedure

To estimate carbonates from either a GRAPE density record or a downhole logging record of wet bulk density, one first decompacts the sediment column and then applies Equation 5 to the corrected density. The decompaction takes into account the porosity loss from burial and resulting change in wet bulk density. The decompaction we applied is listed below, where *mbsf* is the depth below seafloor in meters. The result, D, is the density change as a result of burial:

$$D = 1.2\left(\frac{mbsf}{1000}\right) - 1.374\left(\frac{mbsf}{1000}\right)^2. \quad (6)$$

The decompacted wet bulk density is the measured wet bulk density minus the decompaction. After the decompaction correction was applied, we then adjusted the aluminosilicate characteristic porosity and the aluminosilicate grain density until we had a reasonable fit to measured carbonate values for the core.

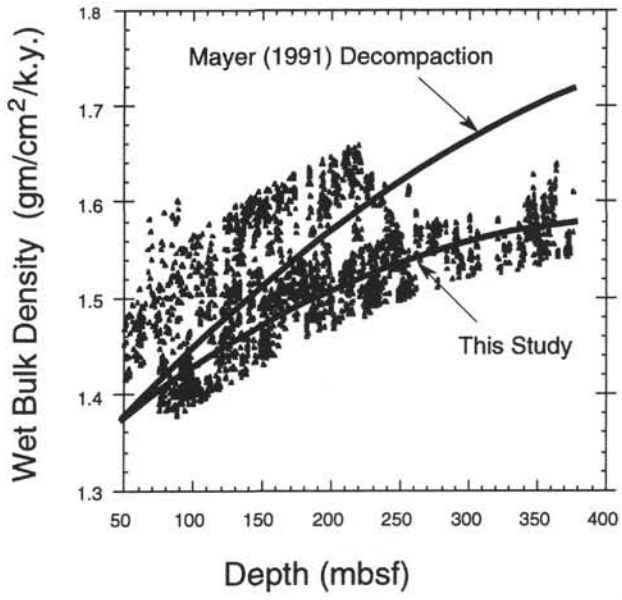

Figure 1. Comparison of Mayer's (1991) compaction curve to one derived empirically for Leg 138. We show data from sediments cored at Sites 844, 846, 848, 850, and 852 that have carbonate contents of 65%–75%. Data from the northern sites (852 and 854) are offset from the near-equatorial sites, which suggests that regional variations in compaction need to be taken into account for the most accurate carbonate predictions from wet bulk density.

We primarily used logging density data to reconstruct carbonates, but in some sites we also used GRAPE data if no logging data were available, or used GRAPE data in the upper part of the section where poor logging data were recorded as a result of bad hole conditions. GRAPE data were used exclusively at Sites 84, 503, 848, 852, and 853. GRAPE data were combined with logging data at Sites 844 (GRAPE data shallower than 120 mbsf) and 849 (GRAPE data shallower than 150 mbsf). In all cases where GRAPE data were used, these were interpolated to either a 10- or 20-cm-sample spacing.

We had little difficulty calibrating carbonate to density for sites where carbonate contents did not vary too dramatically (i.e., where carbonate contents stayed between about 30 and 80%; Sites 84, 503, 847, 848, 849, 850, 851, 852, and 853; Fig. 2). It proved more difficult, however, to match sites that varied through a larger range (Sites 495, 844, 845, 846, and 854). Errors introduced by the simplifying assumptions in the above theory make it difficult to match both carbonate-free sediments and sediments containing more than 70% carbonate (Fig. 3). Nevertheless, reasonable matches were made in all cases except Site 854. We think that the high quantity of ferromanganese oxyhydroxides at the base of the drill site sufficiently altered the density relationships to make the prediction invalid. For this reason, we used only shipboard carbonate data for carbonate MARs at Site 854.

Drill Site Backtracking Methods

Paleoposition

We backtracked the drill sites initially using the modern Cocos/Pacific pole of rotation from DeMets et al. (1990; 36.823°N, 108.629°W, angular rotation (ω) of 2.09 °/m.y.), and used Engebretson et al. (1985) for the Pacific/Nazca and Pacific/hot spot poles of rotation (55.58°N, 90.10°W, ω = 1.42 °/m.y. and 57.00°N, 75.00°W, ω = 0.94 °/m.y., respectively). Changes in absolute movement of the Pacific/hot spot pole of rotation through time are also from Engebretson et al. (1985). Before 5 Ma, the Pacific/hot spot pole was located at 69°N,

Table 2. Modern eastern Pacific surface sediment compositions.

Core name	Water depth (mbsl)	Latitude (°N)	Longitude (°E)	Sed. rate (cm/k.y.)	Bulk MAR (mg/cm²/k.y.)	$CaCO_3$ (%) (XRF)	$CaCO_3$ (%) (LECO)	Calcite free						
								C-org (%)	Norm. opal SiO_2	Al (%)	Si (%)	K (%)	Ti (%)	Fe (%)
OC73-3-7	4247	−17.87	−101.04	0.3	80	17.20	16.30	0.36	10.0	6.90	21.4	2.29	0.405	10.09
Y71-6-16	6761	−16.92	−74.33	5.0	945	0.80	0.70	1.29	32.3	7.24	31.3	2.28	0.401	3.96
Y71-6-26	4813	−15.27	−76.37	0.3	56	1.80	1.50	1.26	33.9	6.94	32.1	2.27	0.389	5.37
Y71-6-8	5273	−13.75	−77.72	0.3	56	0.50	0.40	2.80	41.4	6.25	33.1	1.93	0.369	3.10
KK71-F121	4010	-11.98	−101.48	0.4	243	76.40			32.1	3.60	23.3	1.19	0.311	12.93
Y71-8-55	6309	−11.63	−79.25	2.5	467	0.30	0.70	1.79	39.3	6.63	33.0	1.92	0.367	5.13
Y71-7-47	3188	−11.30	−110.10	1.5	797	88.10			27.5	1.04	15.4	0.10	0.350	25.94
Y71-7-46	3180	−11.17	−110.05	1.0	647	87.60			24.7	1.01	14.0	0.19	0.356	27.34
Y71-7-51F	3209	−11.12	−110.58	1.5	905	65.00			20.9	0.60	11.5	0.44	0.162	28.74
Y71-7-35	3116	−11.10	−110.32	0.3	212	64.80			40.3	4.32	29.5	1.38	0.282	8.88
Y71-7-49	3116	−11.10	−110.32	1.5	821	81.80	82.50	1.85	26.8	1.60	16.3	0.57	0.346	24.34
Y71-7-28	4491	−11.02	−85.02	0.4	130	0.00	0.80	0.51	27.7	8.05	31.6	2.27	0.410	5.42
Y71-7-54	5343	−11.00	−105.75	1.5	280	0.80			18.1	2.14	16.5	0.82	0.194	22.23
KK71-107	3200	−10.98	−107.53	0.4	291	92.30			30.4	3.49	21.8	0.74	0.726	13.27
Y71-7-53	3180	−10.88	−110.73	1.5	282	75.70			28.5	0.68	15.3	0.79	0.191	27.86
Y71-7-38	3691	−10.77	−106.33	0.4	286	89.70			34.5	3.20	23.0	0.73	0.503	14.06
Y71-7-32	3850	−10.75	−93.10	0.8	425	55.40	57.70	0.56	20.8	5.99	24.5	1.85	0.339	7.41
Y71-7-52	3198	−10.72	−110.70	0.3	57	67.50			22.1	0.33	11.5	0.40	0.111	27.87
Y71-7-40	3384	−10.72	−108.23	1.0	662	90.80			13.2	3.51	13.7	0.80	0.968	20.57
Y71-7-44	3167	−10.70	−110.02	1.0	694	83.90			30.0	1.01	16.7	0.47	0.270	24.60
Y71-7-39	3429	−10.70	−108.20	1.0	664	93.90			21.7	3.22	17.1	0.03	1.036	18.30
Y71-7-43	3165	−10.68	−110.00	1.0	690	84.10			26.0	0.89	14.5	0.53	0.298	26.45
AMPH28G	3365	−10.55	−110.87	1.0	573	70.70			22.8	0.55	12.3	0.33	0.137	27.52
AMPH29GV	3205	−10.55	−110.87	1.0	569	70.70			22.4	0.40	11.9	0.40	0.128	27.51
AMPH27P	3090	−10.55	−110.87	1.0	569	71.30			23.6	0.40	12.4	0.49	0.134	27.31
KK71-F165	3810	−10.18	−96.18	1.0	631	79.60			41.9	4.98	30.4	1.31	0.332	7.15
Y71-7-36	4541	−10.13	−102.85	0.4	296	3.20			26.1	2.77	23.0	0.99	0.184	15.06
Y71-7-30	4237	−10.05	−88.68	0.8	377	0.00	0.50	0.51	32.0	7.39	31.9	2.04	0.359	5.36
SCAN93GC	3891	−10.02	−90.08	0.4	99	13.50			29.5	7.44	31.1	2.03	0.355	5.55
Y71-7-35	4010	−9.95	−97.93	0.6	121	65.10			39.9	4.55	29.7	1.39	0.280	8.87
KK71-GC9	4240	−9.95	−93.08	1.0	575	71.60			33.7	6.71	30.5	1.88	0.361	5.06
Y71-7-31	4114	−9.93	−91.97	1.4	889	29.40	30.10	0.90	27.0	7.40	29.9	1.96	0.337	5.76
Y71-7-34	4622	−9.63	−93.33	1.0	530	80.20			35.2	6.47	30.3	1.74	0.376	5.15
Y71-8-61	5843	−9.35	−80.78	3.5	654	0.00	0.40	2.40	42.2	6.30	33.5	1.87	0.361	4.06
AMPH25GC	3660	−9.05	−105.88	0.5	347	88.00	86.90	2.22	44.1	2.28	25.7	0.65	0.407	12.01
C151	4253	−8.97	−86.37	0.3	56	0.00			31.1	7.27	31.5	2.00	0.367	4.96
AMPH24GC	3370	−8.87	−106.42	0.6	432	91.30			41.5	2.39	24.9	0.03	0.637	11.69
C136	4252	−8.78	−89.43	0.4	80	2.80			12.8	8.74	27.3	2.52	0.448	7.42
AMPH23GC	3305	−8.70	−106.90	0.7	507	91.90			40.4	2.44	24.4	0.02	0.678	12.58
AMPH22GC	3240	−8.57	−107.20	0.9	647	91.30			42.9	2.08	25.0	0.00	0.588	12.32
AMPH20PC	3090	−8.48	−107.43	1.0	712	90.40			43.3	1.63	24.5	0.05	0.433	14.88
AMPH21GC	3120	−8.48	−107.43	1.0	701	89.00			49.3	1.34	26.7	0.00	0.389	12.67
RC11-229	3627	−8.35	−111.52	1.7	1123	83.70			40.3	0.74	21.3	0.78	0.259	18.38
AMPH19GC	3090	−8.33	−107.78	1.2	799	84.40			46.8	1.16	24.7	0.38	0.279	17.25
AMPH18GC	3400	−8.18	−108.18	1.3	828	80.40			37.6	0.86	20.0	0.36	0.233	21.80
Y71-8-76	5122	−8.12	−81.60	1.4	945	0.00	0.80	2.69	31.5	7.52	31.2	1.94	0.432	4.41
AMPH17GC	3200	−7.98	−108.62	1.4	915	82.70			47.4	0.77	24.3	0.25	0.210	17.82
AMPH16GC	3240	−7.85	−108.92	1.8	1192	83.90	84.30	1.73	53.6	0.76	27.3	0.26	0.223	14.90
Y71-8-79	6165	−7.83	−81.28	1.6	1022	0.00	0.60	2.06	36.4	7.19	32.6	1.95	0.424	4.16
AMPH15PG	3300	−7.72	−109.33	1.7	1149	85.70			55.7	0.91	28.5	0.16	0.225	13.88
AMPH12GC	3480	−7.60	−110.97	1.1	756	87.20			54.2	0.96	27.9	0.02	0.288	13.44
AMPH14GC	3315	−7.57	−109.77	1.4	933	84.40			60.6	0.87	30.6	0.04	0.227	11.42
V21-35	3939	−7.52	−95.32	1.8	1087	73.00			49.8	4.82	33.5	1.17	0.280	4.83
AMPH11PC	3728	−7.47	−113.53	0.4	252	79.50	80.50	1.00	51.8	1.19	27.3	0.54	0.197	12.97
AMPH13GC	3395	−7.32	−110.97	1.0	665	84.30			55.4	0.85	28.7	0.76	0.223	11.81
OC73-1-2	3160	−7.28	−107.62	1.4	957	86.70	86.10	2.91	54.2	1.29	28.4	0.28	0.397	12.40
Y71-9-92	3350	−6.80	−106.12	1.3	907	85.70	84.20	2.13	73.8	1.02	36.8	0.15	0.220	5.84
Y71-9-93	3521	−6.75	−106.32	1.3	875	85.60			74.4	0.99	37.0	0.09	0.202	6.87
Y71-9-96	3470	−6.65	−106.45	1.2	806	85.30			78.6	0.88	38.7	0.03	0.198	5.87
Y71-9-94	3687	−6.65	−106.28	1.2	791	88.50			52.2	2.11	29.0	0.23	0.335	13.17
Y71-9-97	3319	−6.60	−106.80	2.0	944	83.50			75.5	0.73	37.0	0.23	0.166	7.53
Y71-9-98	3305	−6.52	−106.58			85.10			73.0	0.83	36.0	0.22	0.19	48.13
Y71-9-101	3175	−6.38	−106.52	1.7	1088	85.60			63.7	1.07	32.3	0.19	0.235	11.40
Y71-9-90	3295	−6.13	−102.62	1.2	811	80.40	80.30	0.64	69.8	1.00	35.3	0.52	0.185	7.76
KK71-150	3080	−6.10	−106.72	1.2	797	84.10			74.8	0.87	37.0	0.24	0.172	8.09
Y71-9-104	2988	−6.08	−107.08	1.7	1032	80.70			67.8	0.83	33.8	0.20	0.172	10.78
Y71-9-106	3130	−6.07	−107.12	1.9	1152	80.90			75.3	0.73	37.1	0.20	0.172	8.22
Y71-9-109	3240	−6.05	−107.30	1.9	1051	76.30			67.4	0.60	33.2	0.26	0.140	10.95
Y71-9-89	3990	−5.98	−101.03	1.5	847	74.00			66.0	1.95	35.2	0.50	0.174	7.53
Y71-9-91	3512	−5.95	−104.87	1.3	878	70.10	69.80	1.55	70.5	1.15	35.7	0.35	0.123	7.47
Y71-9-110	3196	−5.93	−107.32	1.4	364	76.20			61.7	0.75	31.4	0.68	0.153	13.24
Y71-9-111	3499	−5.85	−107.48	1.3	593	68.40			75.2	0.53	36.4	0.19	0.091	8.34
V21-40	3182	−5.52	−106.77	1.8	1130	70.40			62.5	0.65	32.5	0.95	0.124	6.17
Y71-9-86	3877	−5.08	−90.77	1.4	828	57.70	60.00	1.55	51.9	4.41	34.0	1.03	0.232	3.28
Y71-9-85	3858	−5.03	−87.45	1.6	961	52.90	55.00	1.65	43.8	6.16	34.0	1.34	0.289	3.65
KK71-79P	3850	−5.02	−89.97	1.4	694	59.40			60.8	4.36	38.3	1.07	0.247	3.28
Y71-9-88	3650	−5.00	−91.43	1.2	764	75.40	76.80	1.39	65.2	1.82	34.4	0.48	0.173	5.94
Y71-9-84	4010	−5.00	−85.95	1.4	679	16.00	18.00	1.32	31.6	7.46	31.8	1.73	0.357	4.98
SCAN92GC	3686	−4.98	−88.07	1.3	676	63.30			53.4	5.15	36.2	1.12	0.259	3.20
Y69-83M1	3759	−4.00	−92.02	3.5	1561	63.70	64.30	1.76	67.0	3.05	38.0	0.85	0.197	3.13
Y69-84M1	3748	−3.98	−91.67	5.6	2747	59.80	60.50	1.85	63.8	3.28	37.1	0.84	0.195	2.87
Y73-3-6	3715	−3.78	−94.15			55.60			76.9	2.17	41.2	0.60	0.150	3.08
TR63-31T	3209	−3.60	−83.95	5.0	1667	30.80	32.30	2.39	39.2	6.62	33.1	1.56	0.348	3.91

Table 2 (continued).

Core name	Water depth (mbsl)	Latitude (°N)	Longitude (°E)	Sed. rate (cm/k.y.)	Bulk MAR (mg/cm²/k.y.)	$CaCO_3$ (%) (XRF)	$CaCO_3$ (%) (LECO)	Calcite free						
								C-org (%)	Norm. opal SiO_2	Al (%)	Si (%)	K (%)	Ti (%)	Fe (%)
PLDS1GC	3176	–3.42	–102.77	1.7	1097	81.60	81.40	2.52	75.5	1.61	38.8	0.31	0.173	3.78
TR163-30T	3240	–3.07	–84.88	3.6	1768	58.70	59.40	2.41	43.5	5.88	33.1	1.50	0.327	3.95
KK71-F218	2975	–2.97	–81.63	5.5	1069	1.70			27.5	7.66	30.9	1.67	0.401	4.82
RIS34GC	3210	–2.77	–85.47	3.2	1705	65.30			45.1	5.54	33.5	1.17	0.306	3.54
TR163-29T	3160	–2.43	–85.75	3.6	1980	67.90			51.2	4.78	34.1	1.21	0.299	3.71
Y69-104M1	3892	–2.30	–81.52	1.8	943	2.10	2.50	3.37	26.2	7.31	29.3	1.58	0.402	4.93
TR163-27T	3180	–2.23	–86.58	3.7	2057	68.80			55.4	4.06	34.6	1.17	0.292	3.56
Y69-86M1	3245	–1.98	–91.67	3.7	849	51.20	51.60	2.05	63.7	2.90	35.9	0.73	0.286	2.52
Y71-3-14	2584	–1.67	–85.80	4.8	2884	71.30	72.80	2.89	55.0	4.36	35.0	1.04	0.297	3.40
TR163-25T	2650	–1.65	–88.45	4.5	2617	72.60	71.90	3.16	65.2	2.93	36.6	0.77	0.324	3.23
KK74-FF17	3352	–0.87	–95.48	2.8	1360	57.80			68.2	1.76	35.5	0.50	0.135	1.74
SCAN91GC	2697	–0.42	–86.32	5.5	3083	69.50	70.60	2.40	41.3	5.33	30.7	1.38	0.315	4.22
KK74-TC2	3333	–0.33	–102.25	2.2	1068	57.80			73.8	0.94	36.5	0.30	0.085	2.57
KK74-TC1	3295	–0.20	–100.37	2.2	1071	58.00			69.6	1.13	34.9	0.33	0.087	2.41
RIS32PG	2770	–0.15	–86.98	6.0	2902	57.50			41.3	4.65	30.2	1.18	0.263	3.40
KK71-F219	2281	–0.02	–82.75	3.7	1280	33.20			34.4	4.89	26.8	1.18	0.253	3.37
KK74-FF1	3140	0.02	–102.22	2.4	1180	58.80			70.9	1.00	35.3	0.42	0.087	2.84
Y69-103M1	1808	0.08	–82.42	3.8	1218	44.10	44.70	2.36	34.6	6.68	30.6	1.57	0.320	3.51
Y69-105M1	3408	0.15	–84.05	1.3	741	28.30	28.70	2.04	36.2	6.08	31.8	1.49	0.273	4.16
Y69-110M1	3083	0.22	–81.10	4.5	862	41.90	46.10	0.76	22.9	7.92	28.8	1.64	0.417	4.49
TR163-23T	2730	0.40	–92.17	5.3	2499	55.50	50.40	1.46	62.0	3.01	35.3	0.60	0.732	4.86
PLDS35G	2781	0.43	–86.10	5.0	2394	56.70			40.2	4.33	28.2	0.88	0.245	3.10
TR163-22T	2830	0.52	–92.38	5.3	2554	57.20	54.80	1.70	64.4	2.94	36.3	0.66	0.555	3.70
Y69-97M1	2362	0.53	–91.63	4.5	2577	58.60	47.00	0.89	38.9	4.67	28.5	0.55	1.363	8.57
Y71-3-31	2840	0.53	–85.70	4.8	2791	79.00	79.90	2.63	46.5	5.35	33.3	1.05	0.339	4.15
PLDS48G	2765	0.58	–86.03	5.0	2468	59.10			44.1	4.37	30.2	0.92	0.249	3.54
TR163-21T	2760	0.60	–93.30	5.0	2747	67.80	64.40	1.89	66.1	2.58	36.2	0.61	0.339	3.03
PLDS18G	2737	0.63	–86.12	5.0	2487	59.70			41.6	4.48	29.3	0.92	0.256	3.64
Y71-3-32	2641	0.72	–85.43	2.0	823	72.60	74.70	2.17	51.1	4.93	34.4	1.09	0.316	3.62
Y71-3-32	2641	0.72	–85.42	2.0	725	75.40	76.90	2.39	48.2	5.33	33.9	1.12	0.338	3.78
TR163-20T	3200	0.79	–93.85	3.9	2155	66.90	68.10	3.00	52.9	4.64	34.5	1.15	0.278	3.22
TR163-20B	3200	0.79	–93.85	3.9	2119	68.30	67.80	2.39	69.4	2.27	37.3	0.73	0.235	3.23
RC13-137	3436	0.85	–96.03	2.7	1387	62.30	59.60	4.31	67.4	2.15	36.4	0.55	0.162	3.17
Y69-76M1	2319	1.00	–92.02	1.8	896	69.70	62.60	2.14	59.1	3.38	34.8	0.58	0.673	4.76
Y69-72M1	2586	1.02	–87.45	4.0	2226	69.70	71.30	2.56	39.6	4.79	28.6	1.20	0.323	4.69
Y71-3-10A	3482	1.22	–82.27	5.5	3445	9.50	10.00	1.78	28.9	7.66	31.1	1.58	0.359	4.74
Y69-73M1	2707	1.45	–87.93	4.0	2237	67.40	67.80	2.17	35.0	4.52	25.9	1.14	0.294	4.01
SCAN96PC	3856	1.48	–113.87	1.3	843	82.00	83.20	1.82	70.7	2.06	37.4	0.52	0.203	2.48
RC13-138	2655	1.82	–94.13	5.0	2887	72.00	67.60	1.60	60.4	2.64	34.6	0.64	0.244	2.64
RC10-56	2082	1.82	–91.25	5.2	3049	73.30	68.20	2.08	40.9	4.21	29.7	0.92	0.512	5.12
Y69-74M1	2586	2.03	–88.32	2.7	1774	68.90	69.20	1.99	33.1	4.64	25.2	1.09	0.300	3.51
Y69-74M2	2586	2.03	–88.32	5.6	3147	69.30	68.90	2.06	35.0	4.83	26.5	1.08	0.305	3.69
TR163-19T	2348	2.27	–90.95	3.0	1967	83.00	80.20	2.89	54.3	4.24	34.3	0.97	0.461	4.82
RIS29GC	2230	2.30	–89.45	2.9	1863	81.20			37.7	5.36	29.7	0.79	0.417	4.57
RC10-63	3468	2.32	–104.45	1.9	1266	84.40	83.30	2.49	58.6	2.77	33.5	0.70	0.255	5.32
KK74-FF12	2947	2.33	–100.77	2.1	1211	71.90			57.9	1.84	31.2	0.50	0.196	5.12
KK74-PC4	3146	2.37	–100.83	2.3	1288	69.40			61.9	1.53	32.3	0.49	0.180	5.22
SCAN84PG	4478	2.47	–121.43	0.7	350	60.10	61.40	1.01	66.1	3.22	37.6	0.80	0.140	2.26
RC13-119	3792	2.53	–107.22	1.7	1090	81.00	78.20	2.50	57.4	2.76	33.0	0.86	0.228	4.17
TR163-18T	2030	2.82	–89.85	2.2	1438	82.70	82.20	2.99	42.6	4.93	30.3	1.14	0.402	7.29
Y69-106M1	2870	2.98	–86.55	1.9	514	63.90	66.40	2.12	29.2	6.51	27.8	1.33	0.366	5.50
RC10-62	3120	3.33	–101.72	1.8	1199	84.40	84.60	2.94	47.0	3.30	29.8	0.91	0.280	10.13
Y69-75M1	2198	3.48	–89.70	1.8	941	83.20	82.40	2.39	35.4	6.05	29.3	1.21	0.451	4.93
SCAN86PG	3441	3.50	–99.47	1.8	1146	80.40	79.50	1.98	44.4	3.46	28.4	0.74	0.281	10.28
Y69-112M1	3848	3.50	–78.95	5.0	937	1.90	0.90	2.60	14.3	9.33	27.4	1.16	0.451	5.77
V28-148	2834	3.80	–91.53	0.9	436	75.80	75.30	2.01	30.2	6.01	27.5	1.30	0.409	4.99
V28-149	2882	3.87	–92.12	0.9	387	79.20	79.60	1.95	28.9	6.20	27.0	1.41	0.428	5.19
RIS15GC	4100	3.95	–118.05	0.7	481	87.20	87.20	2.10	61.7	2.89	35.1	0.63	0.310	4.26
RIS27GC	3150	4.08	–92.17	1.6	920	71.60			26.2	6.43	26.0	1.18	0.411	5.52
Y69-108	3390	4.10	–85.03	3.8	710	18.20	7.90	1.91	22.5	7.07	28.6	1.41	0.406	7.02
TR163-15T	1770	4.27	–87.90	1.4	940	85.10	82.70	4.34	30.3	7.27	29.3	1.07	0.692	5.88
RC10-61	3479	4.32	–99.37			75.90	78.20	2.62	45.2	3.19	27.8	0.71	0.265	9.18
RC10-57	3338	4.35	–93.27	1.5	795	64.80	64.20	1.42	30.2	5.92	28.5	1.25	0.350	6.20
RIS16GC	3970	4.40	–113.72	1.0	619	77.90	77.90	2.28	40.5	4.55	28.7	1.09	0.301	6.07
RIS17GC	4110	4.73	–111.53	1.0	600	75.30	76.50	2.52	41.8	4.32	28.7	1.10	0.272	6.13
Y69-107M1	2716	4.78	–88.48	3.9	1532	70.90	73.30	1.78	25.7	7.14	27.2	1.26	0.477	4.90
RC10-60	3460	4.95	–97.92	1.3	787	76.00	76.20	1.72	40.7	3.94	27.7	1.00	0.285	10.61
RC13-136	3486	4.98	–94.47	1.3	628	57.40	55.70	1.16	29.5	5.90	28.7	1.33	0.345	7.05
RIS18GC	3910	5.00	–109.20	1.0	617	77.70	76.00	2.27	30.5	4.76	25.3	1.00	0.345	8.18
Y69-113M1	3816	5.03	–78.00	7.2	4046	0.20	0.60	2.43	10.4	8.99	26.6	1.38	0.590	7.47
RIS19GC	3720	5.18	–106.60	1.1	695	79.70	79.40	3.11	31.1	4.86	25.0	1.05	0.360	9.94
Y71-3-9	3601	5.25	–81.52	5.0	974	1.30			15.7	8.04	27.7	1.31	0.519	7.63
Y71-3-8	3888	5.32	–81.93	5.0	952	1.00	2.70	2.54	11.6	8.46	27.4	1.28	0.581	6.58
RIS14GC	4330	5.33	–117.92	0.5	291	72.60	74.60	1.83	43.7	5.11	31.4	1.23	0.272	4.72
Y69-111M1	3768	5.50	–81.23	5.0	937	0.00			13.6	8.54	26.9	1.23	0.602	6.59
RIS21GC	3330	5.53	–103.15	1.4	832	74.40	73.30	2.34	26.2	5.35	24.0	1.16	0.357	11.57
RC10-59	3662	5.57	–96.32	1.2	622	63.00	64.00	1.82	35.9	4.71	28.1	1.24	0.286	10.27
RIS20GC	3570	5.58	–104.47	1.4	869	78.20	77.20	3.29	27.7	5.23	24.3	1.10	0.357	11.29
RIS24GC	3310	5.65	–99.93	1.4	752	65.90	67.30	2.51	24.6	5.59	23.9	1.13	0.330	9.67
RIS22GC	3210	5.67	–102.10	1.1	542	58.90	61.50	1.74	24.7	6.55	25.9	1.39	0.356	8.34
TR163-14T	2365	5.90	–87.23	0.9	458	61.60	63.50	1.72	19.2	8.44	27.3	1.51	0.636	5.95
Y71-3-5	2363	5.92	–84.93	2.0	965	36.30	38.60	2.16	16.1	8.64	27.4	1.45	0.601	6.62
RIS23GC	3310	5.93	–101.25	1.0	547	67.40	69.60	2.83	25.3	6.63	26.3	1.30	0.358	8.35

Table 2 (continued).

Core name	Water depth (mbsl)	Latitude (°N)	Longitude (°E)	Sed. rate (cm/k.y.)	Bulk MAR (mg/cm²/k.y.)	$CaCO_3$ (%) (XRF)	$CaCO_3$ (%) (LECO)	Calcite free						
								C-org (%)	Norm. opal SiO_2	Al (%)	Si (%)	K (%)	Ti (%)	Fe (%)
TR163-12T	1765	6.02	–87.37	0.9	559	78.20	79.00	3.89	16.0	9.05	26.9	1.19	0.690	6.20
TR163-13T	2450	6.03	–87.35	0.9	475	64.50	65.80	2.11	21.9	8.34	28.3	1.45	0.597	5.80
RC10-58	3660	6.13	–94.78	0.9	355	42.10	39.50	1.15	29.8	5.95	29.2	1.39	0.335	7.51
TRIP1PC	3626	6.22	–90.83	0.9	174	1.50	2.10	0.51	32.2	6.91	30.3	2.28	0.287	4.10
V20-25	3753	6.35	–106.00	0.8	437	67.40	70.20	1.65	20.5	5.89	23.1	1.39	0.365	11.16
V28-150	3630	6.35	–97.28	0.9	311	57.70	59.80	1.22	26.9	5.23	24.3	1.36	0.324	11.14
Y71-3-6	1945	6.38	–85.37	3.8	727	45.20	47.70	2.14	15.4	8.85	27.4	1.45	0.621	6.71
TR163-11T	1950	6.45	–85.82	1.8	814	52.30	54.40	2.16	15.0	9.05	27.3	1.54	0.618	5.98
KK74-FF76	3535	6.55	–104.90	1.2	685	71.00			36.6	4.83	27.7	1.19	0.301	10.57
V18-346	3543	6.55	–89.97	0.9	170	0.50	1.30	1.50	21.9	7.20	28.1	1.39	0.445	5.26
Y71-3-7	1765	6.57	–85.58	4.0	770	57.30	59.00	2.66	14.5	9.42	28.0	1.44	0.641	6.25
V18-347	3246	6.62	–88.42	0.9	238	17.00	17.80	1.96	17.2	8.02	27.6	1.41	0.553	5.97
RIS25GC	3500	6.63	–97.45	0.9	357	42.50	44.40	1.46	26.3	5.83	25.4	1.28	0.327	9.25
Y69-114M1	3333	6.75	–79.77	7.0	3827	0.20	0.70	3.25	11.5	9.07	26.4	1.14	0.648	6.83
RIS13GC	3970	6.77	–117.87	0.4	226	70.10	72.80	1.59	32.0	6.41	29.2	1.55	0.349	6.09
V28-151	3574	6.87	–98.40	1.2	349	48.50	49.50	1.56	28.5	5.85	26.5	1.64	0.315	9.18
RIS26GC	3680	6.98	–94.95	0.9	198	7.50	7.50	2.45	28.5	5.55	26.4	1.27	0.312	7.93
V18-322	3882	7.20	–111.42	0.4	215	65.90			28.7	5.94	26.8	1.45	0.351	9.21
KK71F220A	1643	7.22	–84.22	3.9	1705	49.70			16.6	7.67	25.2	1.27	0.568	7.10
V28-152	3347	7.30	–100.18	1.4	317	33.20	34.10	1.41	25.3	7.15	28.4	1.66	0.396	6.41
V20-21	3166	7.52	–102.12	1.1	366	30.70	30.60	1.46	23.6	7.62	29.5	1.66	0.399	6.34
TR163-1TW	1700	7.72	–83.08	3.7	739	2.90	2.30	2.86	8.6	8.93	26.2	1.34	0.705	7.08
V20-20	3288	7.73	–101.35	1.0	256	15.10	14.40	1.52	23.2	7.70	29.8	1.63	0.401	5.66
TRIP3GC	3436	7.75	–92.25	1.0	193	1.50	2.10	1.24	33.5	6.60	31.5	1.45	0.396	5.24
KK74-GC2	3319	7.87	–104.25	1.2	547	52.90			34.1	5.37	28.1	1.21	0.304	9.94
V20-16	3336	8.05	–87.03	2.5	472	0.40	0.90	1.66	17.6	8.14	28.8	1.52	0.591	6.12
KK74-GC1	3469	8.08	–104.30	1.2	527	50.00			30.5	5.10	27.1	1.42	0.301	12.20
TR163-9TW	3420	8.08	–89.65	1.3	257	2.50	3.50	1.71	30.4	6.92	31.2	1.48	0.477	5.64
KK74-FF77	3428	8.12	–104.13	1.2	493	45.10			30.4	5.31	26.2	1.25	0.320	10.84
RIS12GC	3930	8.17	–117.88	0.3	163	66.90	68.60	1.83	28.8	7.04	29.6	1.75	0.374	6.02
TR163-2TW	1620	8.25	–84.35	4.2	1060	14.40	15.30	2.45	8.4	8.70	26.2	1.44	0.695	7.06
CCTW1GC	3280	8.27	–104.17	1.2	427	35.00			23.1	6.30	25.3	1.28	0.406	10.14
CCTW2GC	3100	8.27	–104.10	1.2	475	42.50			22.8	6.07	24.4	1.49	0.401	10.43
TR163-7TW	3435	8.37	–88.03	1.8	360	3.00	3.60	1.62	20.6	7.46	28.1	1.49	0.547	6.40
TR163-8TW	3413	8.38	–88.05	1.8	350	1.70	2.10	1.54	27.3	7.22	30.4	1.50	0.498	5.73
RC10-248	3493	8.45	–91.45	2.0	385	1.30	1.30	2.04	30.1	6.31	30.6	1.39	0.390	4.90
RC10-247	3512	8.60	–91.82	2.0	390	1.90	2.00	2.70	34.0	6.13	32.1	1.46	0.380	4.97
PAPA39GC	3647	8.72	–92.40	2.1	399	0.70	1.00	1.25	27.4	6.71	28.7	1.44	0.403	5.34
TR163-6TW	3210	8.73	–86.55	2.5	476	0.80			21.1	7.89	29.3	1.54	0.613	6.85
V18-324	3517	8.77	–107.15	0.4	156	41.20			23.4	5.10	22.9	1.30	0.302	10.00
TR163-5TW	3195	8.78	–85.82	3.2	601	0.20	0.50	0.23	34.7	6.92	30.9	2.39	0.298	2.80
TRIP2PG	3492	8.88	–93.25	1.9	375	2.40	2.60	2.07	36.0	6.17	32.2	1.61	0.346	5.20
TR163-3TW	2950	8.88	–85.23	3.5	692	2.50	2.60	1.82	14.5	8.44	27.9	1.55	0.702	6.96
TR163-4TW	3150	8.88	–85.18	3.5	665	0.70	0.80	0.46	13.6	8.63	28.2	1.59	0.658	6.52
V20-17	3420	9.00	–90.28	3.0	566	0.40	0.60	2.14	31.9	6.51	31.6	1.47	0.435	5.09
V28-153	3272	9.05	–102.67	1.2	228	22.40	22.60	2.22	22.2	7.66	29.1	1.87	0.419	6.10
V28-155	3431	9.63	–101.12	3.7	1499	0.80	1.60	2.04	21.1	7.93	28.9	1.64	0.436	5.62
RC13-134	4098	9.65	–95.38	1.7	324	0.80	0.70	2.00	31.0	6.25	32.7	1.46	0.342	6.66
V28-156	3702	9.68	–99.98	5.5	1078	0.30	1.10	1.77	26.4	7.63	30.7	1.72	0.412	5.77
RC10-246	3884	9.68	–95.33	1.7	318	0.10	1.00	2.23	25.6	5.97	31.4	1.65	0.343	7.00
V20-18	3656	9.87	–92.53	3.2	620	1.60	1.40	2.47	27.7	7.23	30.7	1.59	0.453	5.38
PAPA4GC	4321	9.93	–119.70	0.2	43	6.40			26.9	7.75	31.1	2.41	0.411	5.42
V28-154	3389	9.93	–101.75	1.2	226	8.80	8.10	1.44	24.0	7.81	30.5	1.89	0.421	5.70
RC13-133	3797	10.02	–94.03	2.3	475	4.40	4.00	2.94	26.2	7.35	29.7	1.61	0.470	5.98
TRIP4GC	3847	10.20	–94.43	2.3	447	1.70	1.50	1.67	30.4	6.66	31.1	1.49	0.400	6.35
BNFC20PG1	4240	10.57	–108.38	0.4	77	1.10			23.5	7.00	27.2	1.71	0.390	7.86
PAPA72GC	4010	10.57	–95.37	2.2	426	1.50			30.2	6.36	31.6	1.48	0.375	6.72
BNFC8PG	3441	10.98	–108.53	0.4	179	51.30	54.60	1.26	23.8	7.20	27.1	1.73	0.407	7.00
RC10-245	3680	11.13	–98.73	1.3	243	0.00	1.10	1.24	20.3	8.23	30.5	1.65	0.388	4.26
BNFC17PG1	3522	11.18	–109.62	0.3	141	55.30			30.2	7.44	30.7	1.67	0.573	6.60
TRIP4PG	4141	11.67	–95.38	2.7	507	0.20	0.90	2.10	29.6	6.96	30.1	1.55	0.397	6.45
TRIP5GC	4039	12.63	–96.21	2.0	375	0.10	1.00	1.73	25.4	7.87	30.0	1.73	0.410	4.78
RC13-125	3382	12.75	–101.20	4.1	773	0.40	1.20	2.46	16.9	8.85	29.5	2.02	0.446	5.86
RC13-122	3517	12.83	–107.15	0.6	145	12.20	13.60	1.44	20.7	7.39	28.3	1.84	0.395	6.84
RC13-124	3455	12.83	–100.53	4.2	785	0.00	0.50	1.50	21.5	8.36	29.2	2.32	0.386	5.80
PAPA88GC	3375	13.75	–98.50	4.0	753	0.30	0.60	1.89	16.2	9.16	28.5	2.04	0.454	5.61
RIS9GC	4010	13.92	–117.40	0.2	37	0.00	0.70	0.61	30.1	7.35	31.8	2.47	0.419	5.40
RIS8PG	4065	14.43	–117.20	0.2	37	0.00	0.40	0.63	22.1	7.81	29.6	2.53	0.436	6.06
TRIP6GC	3757	14.43	–108.40	0.7	132	0.50	0.90	0.52	18.1	8.81	28.8	2.21	0.448	6.74
TRIP7GC	3644	14.47	–111.83	0.3	76	14.90	15.40	0.70	19.6	8.44	28.6	2.26	0.429	6.05
BNFC4GC	3268	14.52	–106.03	1.0	191	1.00	1.00	1.23	19.2	7.98	26.9	2.02	0.415	7.79
PAPA99GC	3483	14.52	–102.03	4.4	838	0.80	1.50	1.33	9.1	8.42	23.6	1.74	0.412	9.42
PAPA3GC	4218	14.80	–119.87	0.2	37	0.00			20.4	8.13	29.4	2.61	0.461	5.99
TRIP5PG	3929	15.63	–112.95	0.3	57	0.20	0.80	1.23	18.2	8.18	28.0	2.22	0.425	5.99
TRIP6PG	3438	16.78	–113.00	0.4	86	6.10	6.30	0.48	20.8	8.37	29.1	2.33	0.452	6.47
PAPA103G	3052	17.45	–104.80	3.5	654	0.00			13.5	8.90	26.8	2.03	0.437	8.42
TRIP7PG	3697	17.50	–113.00	0.4	75	0.20	0.80	0.68	20.9	8.23	29.1	2.28	0.454	6.23
KK74-GC4	3935	17.87	–104.22	3.0	571	0.80			11.7	9.80	28.0	2.05	0.519	5.94
BNFC1GC	4200	18.30	–104.67	2.8	587	5.10			10.4	9.69	26.5	1.52	0.601	5.51
TRIP8PG	3463	20.83	–112.52	0.7	133	0.70	0.60	0.32	16.7	8.88	29.0	2.60	0.496	6.07

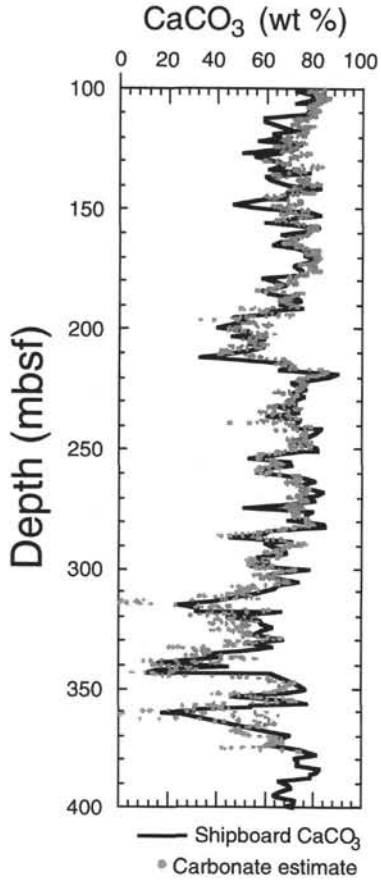

Figure 2. Comparison of carbonate content estimated using Equations 5 and 6, with carbonate measured on board the ship at Site 850. This site has a relatively small range in carbonate content and illustrates sites where density estimates of carbonate proved easy to calibrate with shipboard measurements.

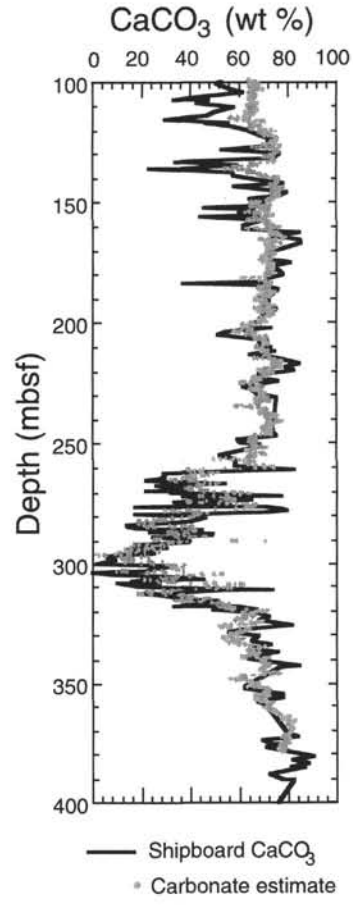

Figure 3. Comparison of carbonate content estimated using Equations 5 and 6, with carbonate measured on board the ship at Site 846. This site has a large range in carbonate content (0%–90%) and calibration of density carbonate estimates to measured carbonate content was more difficult. Nevertheless, density-derived carbonate estimates are comparable to shipboard measurements.

71°W, and $\omega = 0.787$ °/m.y. Backtracked positions at 1-m.y. intervals are listed in Table 3.

We found that backtracked paths for drill sites on the Cocos Plate (Sites 503 and 84) would cross those from drill sites on the Nazca Plate (Sites 504 and 847) if the modern motion of the Cocos Plate had continued unabated since the middle Miocene. For this reason, we decided that Cocos Plate motion prior to 4 Ma was significantly different from modern motion. We assumed that the location for the Pacific/Cocos pole of rotation was 15° eastward and 20° northward of its modern position, and the angular rotation about the pole was 1.30 °/m.y. This radical change in the motion of the Cocos Plate before 4 Ma fits with other reconstructions in progress (Wilson, 1993).

Even with this change, Cocos Plate drill sites still backtracked onto the Pacific Plate (Sites 495, 844, and 845; Fig. 4). We are reluctant to slow Cocos Plate motion further, however, because eastward ridge jumps along this portion of the EPR have occurred in the late Miocene (Mammerickx and Klitgord, 1982; Mammerickx and Naur, 1988). We postulate that these ridge jumps can account for much of the apparent crossover of the site backtrackings.

Paleobathymetry

We calculated changes in depth through time for each site by assuming that all sites have followed a descent away from the rise crest proportional to the square root of time. We assumed that all sites that were formed at the EPR (Sites 495, 572, all Leg 138 sites) had an initial depth of 2900 m below sea level (mbsl), while those formed at the Galapagos Spreading Center (84, 503) formed at an initial water depth of 2600 mbsl. We also corrected for changes in depth from sediment deposition. Bathymetric changes for all drill sites are listed in Table 3.

Age Models

Age models for the Leg 138 drill sites were provided by N. Shackleton (this volume). These time scales were developed by establishing an orbitally tuned time scale for a master sequence and by correlating density events and micropaleontological stratigraphic datum levels between cores. Time scales used in this study were imposed on DSDP cores by choosing a few common microfossil datum levels for initial stratigraphic ties and then by correlating density records from the drill site to nearby Leg 138 cores. The age models then were checked by comparing how well the new age/depth model predicted the positions of biostratigraphic data not used in the original construction (Fig. 5). We used the *Analyseries CFR* Macintosh software package from the Centre des Faibles Radioactivité to correlate between drill sites and to interpolate age scales onto depth sections.

Carbonate MAR Estimates

We estimated average carbonate MARs by using Equation 5 to calculate carbonate values for decompacted density sections, and also

Table 3. Carbonate MARs and paleobathymetry of drill sites.

Age (Ma)	Paleodepth (mbsl)	Backtracked latitude (°N)	Backtracked longitude (°E)	Wet density (g/cm^3)	Porosity (%)	$CaCO_3$ (wt%)	Sed. rate (cm/k.y.)	$CaCO_3$ MAR (g/cm^2/k.y.)
DSDP84								
5.0	2982	1.26	−85.65	1.48	69	57.0	1.54	0.41
5.5	2962			1.48	67	41.5	1.54	0.31
6.0	2940	1.01	−86.50	1.37	72	16.3	2.15	0.13
6.5	2914			1.39	74	49.6	2.32	0.41
7.0	2883	0.74	−87.30	1.49	68	55.0	2.57	0.68
7.5	2844			1.43	71	47.5	2.86	0.56
8.0	2793	0.49	−88.11	1.51	67	60.4	1.79	0.53
8.5	2708			1.50	67	49.9	1.47	0.36
DSDP319								
5.0	4028	−11.92	−107.38	1.30	81	60.7	0.22	0.03
5.5	3997			1.30	81	62.5	0.37	0.06
6.0	3964	−11.59	−108.51	1.30	81	58.5	0.37	0.05
6.5	3931			1.30	81	60.8	0.37	0.06
7.0	3896	−11.24	−109.62	1.30	81	63.2	0.37	0.06
7.5	3859			1.30	81	65.5	0.37	0.06
8.0	3821	−10.86	−110.71	1.30	81	77.5	0.37	0.07
8.5	3781			1.37	79	80.8	0.37	0.09
9.0	3739	−11.21	−110.00	1.45	75	80.5	0.37	0.11
9.5	3694			1.54	72	80.2	0.37	0.13
10.0	3646	−11.56	−109.30	1.60	69	80.0	0.37	0.15
10.5	3594			1.60	69	84.0	0.37	0.15
11.0	3537	−11.89	−108.58	1.60	69	83.1	0.37	0.15
11.5	3475			1.63	66	93.7	3.54	1.85
12.0	3404	−12.23	−107.87	1.67	60	94.4	3.54	2.21
12.5	3319			1.72	58	92.3	3.54	2.38
13.0	3211	−12.55	−107.15	1.69	60	92.1	3.54	2.21
DSDP495								
5.0	4038	9.03	−92.95	1.35	77	3.3	1.66	0.02
5.5	4026			1.35	82	4.5	1.67	0.02
6.0	4015	8.93	−93.69	1.35	83	10.5	1.67	0.04
6.5	4002			1.33	81	19.2	1.29	0.05
7.0	3990	8.80	−94.38	1.34	78	44.9	0.86	0.11
7.5	3977			1.30	79	33.0	0.86	0.08
8.0	3963	8.69	−95.07	1.31	79	34.4	0.71	0.07
8.5	3949			1.29	80	27.3	0.83	0.06
9.0	3935	8.60	−95.76	1.29	80	29.9	1.09	0.08
9.5	3921			1.29	80	24.3	0.96	0.06
10.0	3905	8.52	−96.46	1.28	80	23.6	0.94	0.06
10.5	3890			1.31	79	33.1	1.41	0.13
11.0	3874	8.46	−97.16	1.28	79	11.0	1.28	0.04
11.5	3857			1.46	72	68.7	1.28	0.36
12.0	3840	8.42	−97.85	1.45	72	68.3	1.21	0.34
12.5	3822			1.46	72	68.6	1.43	0.40
13.0	3803	8.39	−98.55	1.52	69	77.9	0.77	0.28
DSDP503								
5.0	3299	1.35	−98.62	1.28	82	40.9	3.45	0.33
5.5	3240			1.29	81	45.9	3.57	0.40
6.0	3174	1.35	−99.47	1.33	79	50.0	6.15	0.87
6.5	3094			1.31	79	36.1	5.54	0.55
7.0	2994	1.33	−100.26	1.39	75	54.6	4.48	0.85
7.5	2847			1.35	76	41.9	2.86	0.38
DSDP572								
5.0	3784	−0.94	−110.19	1.52	69	80.0	2.09	0.79
5.5	3770			1.42	74	68.0	1.94	0.49
6.0	3755	−1.38	−109.44	1.46	72	72.0	2.13	0.63
6.5	3739			1.50	69	73.2	9.19	3.09
7.0	3721	−1.76	−108.76	1.47	71	64.5	8.84	2.45
7.5	3703			1.59	64	77.7	3.00	1.33
8.0	3684	−2.12	−108.07	1.65	61	82.0	4.15	2.19
8.5	3664			1.60	63	76.1	4.52	2.03
9.0	3642	−2.47	−107.38	1.49	68	57.6	2.82	0.78
9.5	3618			1.47	69	52.4	1.57	0.37
10.0	3593	−2.82	−106.68	1.57	64	68.3	2.76	1.05
10.5	3565			1.52	66	58.3	2.65	0.79
11.0	3535	−3.15	−105.98	1.66	60	78.8	0.95	0.50
11.5	3502			1.61	62	73.1	7.26	3.24
12.0	3465	−3.47	−105.27	1.65	60	76.1	6.18	3.12
12.5	3424			1.64	61	76.0	6.77	3.31
13.0	3376	−3.79	−104.56	1.63	61	73.2	5.35	2.47
ODP844								
5.0	3373	4.44	−92.99	1.32	77	25.0	0.41	0.03
5.5	3368			1.33	77	27.4	0.43	0.04
6.0	3362	4.33	−93.80	1.35	76	36.3	0.65	0.08
6.5	3356			1.39	74	45.7	0.41	0.07
7.0	3350	4.21	−94.55	1.43	72	53.4	0.53	0.11
7.5	3343			1.36	75	33.3	0.77	0.09
8.0	3336	4.10	−95.32	1.38	74	35.0	0.95	0.12
8.5	3328			1.43	72	49.3	0.74	0.15
9.0	3320	4.01	−96.08	1.34	76	22.0	0.45	0.03

Table 3 (continued).

Age (Ma)	Paleodepth (mbsl)	Backtracked latitude (°N)	Backtracked longitude (°E)	Wet density (g/cm^3)	Porosity (%)	$CaCO_3$ (wt%)	Sed. rate (cm/k.y.)	$CaCO_3$ MAR (g/cm^2/k.y.)
9.5	3312			1.33	76	17.0	0.79	0.04
10.0	3303	3.94	–96.84	1.37	74	28.1	1.14	0.11
10.5	3293			1.45	70	48.3	1.23	0.25
11.0	3283	3.88	**–97.61**	1.47	69	48.4	2.13	0.47
11.5	3272			1.60	63	75.3	3.12	1.38
12.0	3260	3.84	**–98.37**	1.55	66	70.4	2.94	1.09
12.5	3248			1.56	65	65.9	2.90	1.04
13.0	3234	3.82	**–99.14**	1.57	65	70.2	3.88	1.50
ODP845								
5.0	3611	6.67	**–96.88**	1.20	88	11.4	0.95	0.02
5.5	3600			1.17	90	2.9	1.53	0.01
6.0	3588	6.64	**–97.65**	1.19	90	12.6	1.38	0.02
6.5	3576			1.18	90	8.6	1.22	0.01
7.0	3564	6.59	**–98.37**	1.30	79	27.1	1.08	0.08
7.5	3550			1.29	79	19.3	1.48	0.08
8.0	3536	6.56	**–99.10**	1.30	78	22.0	1.38	0.09
8.5	3522			1.30	78	15.4	1.79	0.08
9.0	3506	6.55	**–99.82**	1.29	78	0.0	1.75	0.00
9.5	3490			1.30	77	6.4	1.19	0.02
10.0	3473	6.55	**–100.54**	1.30	77	3.3	1.25	0.01
10.5	3455			1.36	75	31.1	1.20	0.13
11.0	3435	6.57	**–101.27**	1.40	73	42.4	1.44	0.23
11.5	3415			1.48	70	64.3	1.90	0.54
12.0	3393	6.61	**–101.99**	1.50	69	65.8	2.24	0.68
12.5	3369			1.53	67	70.6	2.60	0.93
13.0	3343	6.66	**–102.71**	1.53	67	68.8	3.09	1.07
ODP846								
5.0	3290	**–2.87**	–96.29	1.52	68	72.6	3.24	1.16
5.5	3288			1.51	68	70.4	2.41	0.81
6.0	3286	**–2.75**	–97.33	1.52	68	69.1	4.43	1.49
6.5	3283			1.51	68	67.1	3.05	0.97
7.0	3280	**–2.61**	–98.39	1.54	66	70.1	3.06	1.12
7.5	3277			1.46	70	56.6	2.90	0.72
8.0	3274	**–2.45**	–99.43	1.42	72	48.7	1.75	0.33
8.5	3270			1.43	72	48.0	1.44	0.28
9.0	3265	**–2.26**	–100.45	1.38	74	33.1	1.94	0.23
9.5	3260			1.35	76	33.2	1.43	0.15
10.0	3255	**–2.04**	–101.45	1.38	74	29.2	1.43	0.15
10.5	3249			1.41	72	41.0	1.17	0.19
11.0	3242	**–1.80**	–102.44	1.44	71	46.9	1.99	0.40
11.5	3234			1.50	68	61.1	1.79	0.53
12.0	3226	**–1.54**	–103.40	1.51	67	62.0	1.80	0.55
12.5	3217			1.57	64	68.8	1.80	0.69
13.0	3206	**–1.25**	–104.35	1.56	65	67.9	1.80	0.67
ODP847								
4.5	3357			1.45	72	71.4	4.52	1.30
5.0	3357	0.88	**–100.75**	1.52	69	78.7	3.80	1.41
5.5	3357			1.46	72	69.1	4.19	1.20
6.0	3356	1.08	**–101.78**	1.49	70	69.7	5.27	1.64
6.5	3354			1.54	67	74.9	5.32	2.01
ODP848								
5.0	3632	**–5.12**	–106.61	1.53	68	79.9	1.31	0.51
5.5	3604			1.46	72	71.1	1.75	0.51
6.0	3575	**–5.50**	–105.81	1.48	70	72.7	1.12	0.36
6.5	3544			1.52	68	77.2	1.11	0.41
7.0	3512	**–5.83**	–105.11	1.64	62	86.7	0.97	0.52
7.5	3477			1.58	65	81.2	0.69	0.30
8.0	3440	**–6.15**	–104.39	1.59	64	82.9	0.43	0.20
8.5	3399			1.61	64	83.6	0.57	0.28
9.0	3355	**–6.46**	–103.68	1.49	70	71.0	0.67	0.22
9.5	3304			1.44	72	62.2	0.59	0.15
10.0	3245	**–6.77**	–102.96	1.52	68	74.0	0.55	0.20
10.5	3173			1.61	64	83.2	0.55	0.27
11.0	3069	**–7.06**	–102.23	1.62	63	83.1	0.59	0.30
ODP849								
5.0	3673	**–1.99**	–106.77	1.56	66	80.3	4.12	1.76
5.5	3650			1.52	68	74.6	5.54	1.98
6.0	3626	**–2.39**	–106.00	1.56	66	77.4	6.89	2.84
6.5	3601			1.50	69	66.3	5.26	1.63
7.0	3573	**–2.73**	–105.31	1.58	65	74.3	5.14	2.13
7.5	3542			1.60	63	76.9	3.00	1.36
8.0	3509	**–3.06**	–104.61	1.63	62	79.2	2.18	1.07
8.5	3473			1.63	62	78.8	1.92	0.95
9.0	3432	**–3.38**	–103.90	1.54	66	67.4	1.80	0.64
9.5	3385			1.42	70	30.4	1.54	0.20
10.0	3330	**–3.70**	–103.19	1.50	68	57.5	1.32	0.36
10.5	3264			1.53	66	61.8	1.57	0.50
11.0	3175	**–4.00**	–102.48	1.48	68	50.2	2.85	0.67
ODP850								
5.0	3649	**–0.90**	–106.82	1.51	69	80.8	3.24	1.21

Table 3 (continued).

Age (Ma)	Paleodepth (mbsl)	Backtracked latitude (°N)	Backtracked longitude (°E)	Wet density (g/cm^3)	Porosity (%)	$CaCO_3$ (wt%)	Sed. rate (cm/k.y.)	$CaCO_3$ MAR (g/cm^2/k.y.)
5.5	3630			1.49	70	74.2	5.50	1.80
6.0	3609	**-1.30**	-106.06	1.53	68	76.1	7.24	2.71
6.5	3587			1.46	71	62.0	5.69	1.50
7.0	3563	**-1.64**	-105.37	1.53	67	70.4	5.92	2.12
7.5	3538			1.55	66	71.4	3.47	1.30
8.0	3509	**-1.98**	-104.67	1.56	65	72.2	3.70	1.44
8.5	3478			1.56	65	70.6	3.31	1.28
9.0	3443	**-2.30**	-103.97	1.53	67	65.1	3.19	1.06
9.5	3404			1.46	69	45.3	3.01	0.62
10.0	3358	**-2.62**	-103.27	1.47	69	47.7	3.18	0.70
10.5	3305			1.49	67	48.8	4.11	0.98
11.0	3238	**-2.93**	-102.56	1.50	67	53.2	4.46	1.18
ODP851								
5.0	3615	0.55	**-106.93**	1.52	69	81.7	2.78	1.07
5.5	3595			1.48	71	76.6	3.10	1.02
6.0	3575	0.14	**-106.19**	1.52	69	78.7	4.33	1.61
6.5	3552			1.47	71	71.3	3.93	1.19
7.0	3529	**-0.21**	-105.50	1.54	67	77.7	4.06	1.59
7.5	3503			1.49	70	69.6	2.48	0.78
8.0	3475	**-0.55**	-104.81	1.54	67	75.5	2.95	1.14
8.5	3444			1.55	66	74.7	2.24	0.87
9.0	3410	**-0.88**	-104.12	1.50	69	66.6	3.50	1.08
9.5	3372			1.43	71	50.5	2.12	0.44
10.0	3329	**-1.20**	-103.42	1.45	71	53.7	2.68	0.61
10.5	3277			1.48	69	54.6	3.78	0.94
11.0	3214	**-1.51**	-102.71	1.47	69	46.7	4.22	0.90
11.5	3128			1.62	62	77.4	2.44	1.15
12.0	2900	**-1.81**	-102.01	1.57	64	71.9	2.32	0.93
ODP852								
5.0	3626	3.06	**-106.55**	1.56	66	81.3	1.59	0.68
5.5	3597			1.51	69	74.7	1.20	0.42
6.0	3566	2.65	**-105.82**	1.57	66	80.4	1.62	0.70
6.5	3533			1.53	68	76.1	1.29	0.48
7.0	3498	2.30	**-105.15**	1.60	64	82.0	1.25	0.59
7.5	3460			1.55	66	76.5	1.09	0.43
8.0	3418	1.95	**-104.47**	1.60	64	81.1	1.71	0.80
8.5	3372			1.64	62	83.7	1.19	0.62
9.0	3320	1.62	**-103.78**	1.49	69	65.4	0.62	0.19
9.5	3260			1.53	62	33.4	0.31	0.06
10.0	3184	1.29	**-103.09**	1.47	70	62.0	0.89	0.25
10.5	3076			1.48	69	62.8	0.86	0.24
ODP853								
5.0	3441	4.97	**-106.31**	1.48	71	73.7	0.79	0.25
5.5	3404			1.44	73	69.1	0.82	0.22
6.0	3363	4.56	**-105.60**	1.53	68	79.0	1.12	0.43
6.5	3318			1.51	69	77.6	1.14	0.42
7.0	3267	4.20	**-104.93**	1.53	68	77.6	1.11	0.42
7.5	3206			1.48	70	71.6	1.15	0.36
8.0	3128	3.85	**-104.27**	1.55	67	79.3	1.54	0.64
8.5	2994			1.57	65	77.7	1.25	0.53
ODP854								
5.0	3372	8.94	**-106.35**	1.40	73	48.3	0.02	0.00
5.5	3347			1.41	73	49.9	0.04	0.01
6.0	3320	8.51	**-105.68**	1.39	74	43.3	0.52	0.08
6.5	3291			1.34	76	27.6	0.39	0.03
7.0	3259	8.14	**-105.04**	1.32	77	20.3	0.95	0.06
7.5	3224			1.29	79	14.2	1.16	0.05
8.0	3184	7.78	**-104.40**	1.33	76	19.2	1.32	0.08
8.5	3136			1.33	74	2.3	0.38	0.00
9.0	3076	7.43	**-103.74**	1.35	72	0.0	0.62	0.00
9.5	2972			1.40	68	0.0	0.53	0.00

used wet bulk density relationships to estimate the water content of the sediment. We used the measured (not decompacted) density at each depth and the sedimentation rate to calculate the carbonate MAR. Time spans of 0.5 Ma were averaged, and all data are reported in Table 3.

RESULTS

Modern Eastern Pacific

Sedimentation patterns within the modern eastern Pacific Ocean have been described in more detail in Lyle (1992). Here, we outline details of modern carbonate deposition so that we can contrast these patterns with those of the late Miocene. The relevant core top data are found in Table 2, as well as data for the maps in Lyle (1992). Figure 6 shows the locations of DSDP and ODP drill sites in the eastern Pacific and indicates the basins in the region. Although the Bauer and Peru basins are distinct and separated by the fossil Galapagos Rise, we have combined data from the two and report all as from the Peru Basin.

Eastern Pacific CCDs

Each basin east of the EPR has a distinctive CCD, partly because the basins are isolated from the main Pacific basin by the rise crest, and partly because each has a different downward flux of CO_2 from different average levels of primary productivity in the surface waters over them. Figure 7 illustrates the different CCD levels in the different eastern Pacific basins. Note that the figure is expressed in carbonate MAR, a more reliable way to measure carbonate dissolution than by

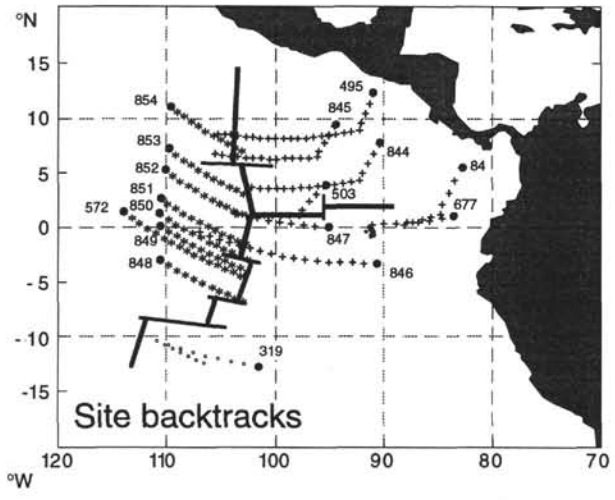

Figure 4. Site backtracked paths used here, shown at 1 Ma intervals. Site backtrackings on the Cocos Plate apparently crossed to the Pacific Plate because of a ridge jump during the late Miocene.

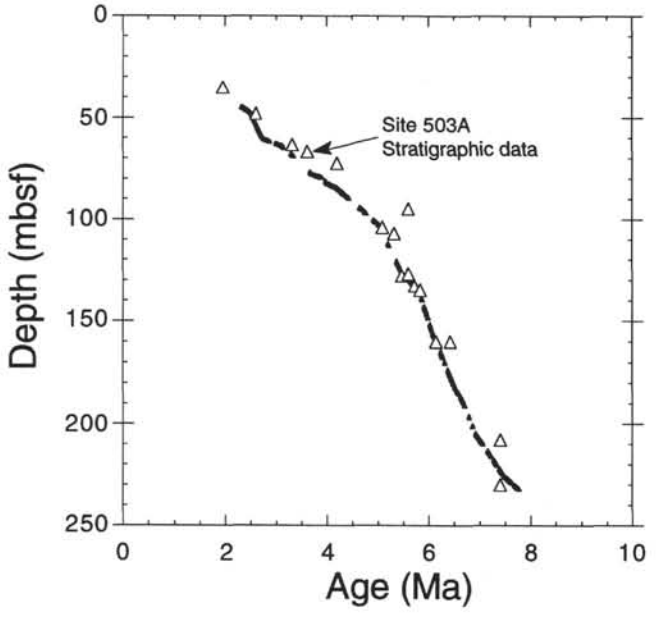

Figure 5. Age/depth model for Hole 503A. The large triangles are microfossil datum levels reported in the *Initial Reports* volume, with ages calibrated to Shackleton's Leg 138 age model. The trace marks the correlation between density records of Site 503 and Site 846.

using sedimentary carbonate content. We define the CCD based on MAR to be where carbonate accumulation is less than 100 mg/cm^2/k.y. By this definition, the Panama Basin has a CCD at about 3300 mbsl, the Guatemala Basin's CCD is at 3600 mbsl, the Peru Basin CCD is at 4100 mbsl, and that of the Pacific Basin proper in the eastern equatorial region, is about 4500 mbsl.

Eastern Pacific AOU

Lonsdale (1976) described circulation patterns in the southeastern Pacific Ocean, and demonstrated that different mid-ocean ridge segments and aseismic ridges isolate waters in each of the eastern Pacific Basins. Deep water in the Peru Basin primarily comes from the south, across first the Chile Ridge and then through gaps in the Sala y Gomez/Nazca Ridge Complex. Deep-water influx to the Panama

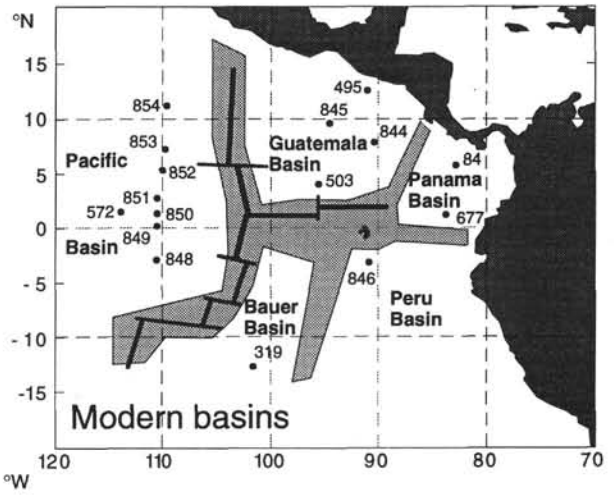

Figure 6. Locations of the different basins in the eastern Pacific and modern locations of ODP and DSDP drill sites in the region. Cross-hatchured regions mark the modern mid-ocean ridge crests, the aseismic Cocos Ridge (between the Galapagos Islands and Panama), the Carnegie Ridge (between the Galapagos Islands and Ecuador), the Galapagos Platform, and the fossil Galapagos Rise.

Basin travels from the Peru Basin along the Peru-Chile Trench past the Carnegie Ridge (the east-west ridge along the equator to South America, Fig. 6) as well as over a saddle in the central Carnegie Ridge. In contrast, bottom waters in the Guatemala Basin cross the EPR near the triple junction with the Galapagos Spreading Center, circulate around the basin, and leave across the EPR to the north (Lonsdale, 1976; Lyle, 1992). The relatively shallow sills prevent true Pacific deep waters from entering the eastern Pacific region east of the EPR. Instead, waters of mid-depth origin fill these basins.

The deep waters in each eastern Pacific basin have characteristic O_2 contents, and with knowledge of deep-water flow paths, an average apparent oxygen utilization (AOU) for each basin can be calculated. AOU is a direct measure of C_{org} degradation and CO_2 addition by productivity in each basin. Pacific deep waters at the equator west of the EPR have 3.2 mL O_2/L. Deep waters of the Peru Basin also have 3.2 mL O_2/L, less than the value of 3.5 mL O_2/L found south of the Nazca Ridge along the deep-water flow path (Lonsdale, 1976). In contrast, Panama Basin deep waters have only 2.5 mL O_2/L (Lonsdale, 1976), and Guatemala Basin deep waters have about 2.75 mL O_2/L (WOCE, unpubl. data). The Peru Basin thus has an AOU of 0.3 mL O_2/L (the difference in O_2 content between the Chile and Peru basins), Panama Basin has an AOU of 0.7 mL O_2/L (Peru–Panama Basin), and Guatemala Basin has an AOU of 0.45 mL O_2/L (Pacific–Guatemala Basin).

Figure 8 shows a comparison of AOU to CCD levels in each of the eastern Pacific basins. The good correlation between the two is evidence that the different CCDs found in each eastern Pacific basin are maintained by different levels of deep CO_2 storage from C_{org} degradation. The regression predicts a CCD rise of 1780 m for each milliliter of O_2/L consumed in deep waters.

Primary Productivity and CCD

The correlation between AOU and CCD does not necessarily mean a strong correlation between productivity and CCD. AOU can increase either by increases in productivity or by slowing deep-water passage through the basins. In the modern eastern Pacific, however, the correlation of CCD depth and productivity suggests that the link between the two is strong. For example, during 1967 to 1968 (Love, 1972; Love and Allen, 1975), the highest annual productivity was found in surface waters over the Panama Basin, followed by the

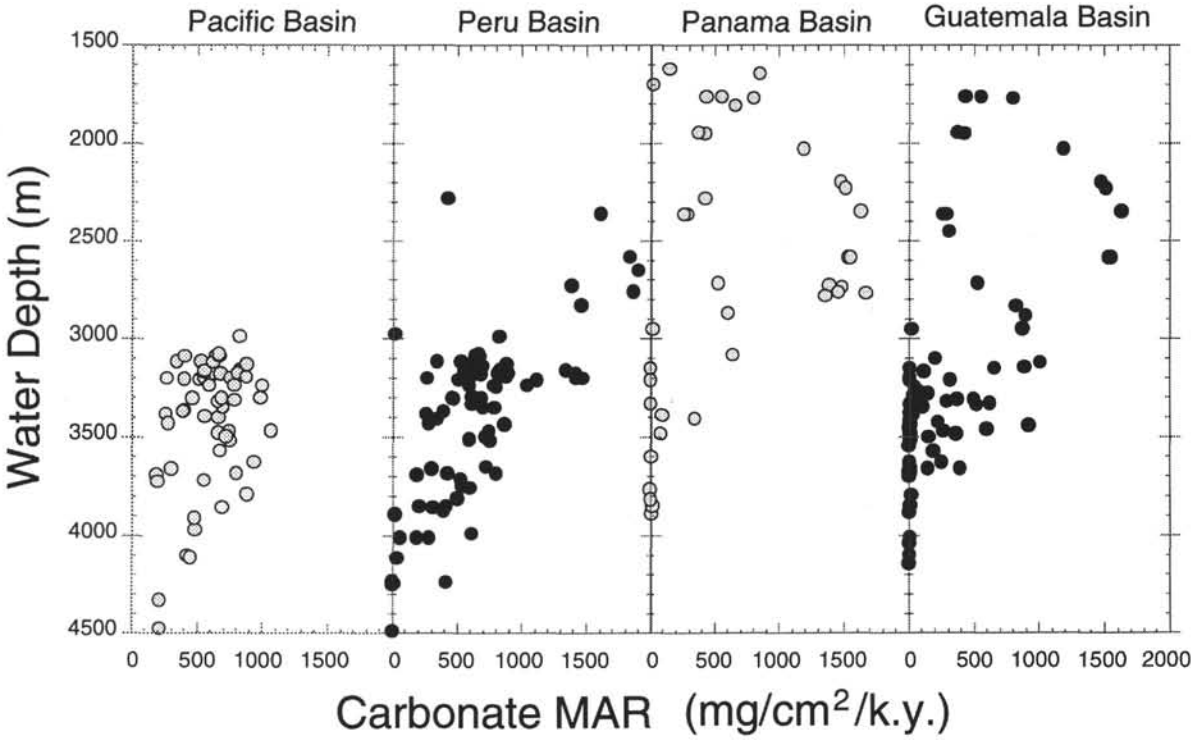

Figure 7. Carbonate compensation depths for the eastern Pacific basins. CCD is defined as carbonate deposition less than 100 mg/cm^2/k.y. The Panama Basin CCD is 3300 m, Guatemala Basin CCD is 3600 m, Peru Basin CCD is 4100 m, and the Pacific Basin proper has a regional CCD of about 4500 m.

Guatemala Basin, the Peru Basin, and the Pacific Basin, in the same order as the relative CCD depths or AOU. The relationships between productivity, AOU, and CCD mean that one can roughly estimate how CCD should respond to changes in productivity.

The CCD in the Guatemala Basin is 3600 mbsl, while that of the Panama Basin is about 3300 mbsl, a 300-m difference. Based upon Koblenz-Mishke (1965), the average productivity of the Guatemala Basin is roughly half that of the Panama Basin. If all the change in CCD is caused by the productivity difference between the two basins, a doubling of productivity causes a rise in the CCD of 300 m.

Emerson and Bender (1981) independently estimated that the CCD could rise by about 200 m if the ratio of C_{org} to C_{CO_3} in particulate rain from surface waters doubled. C_{org}:C_{CO_3} measured in sediment traps is correlated with C_{org} rain (Karlin et al., 1992), which is in turn strongly correlated with surface productivity. Thus, if Emerson and Bender (1981) were correct and the sediment trap measurements are typical, doubling productivity will double the C_{org}:C_{CO_3} in falling particulate matter, and in turn will cause a CCD rise of about 200 m. The approach of Emerson and Bender (1981) thus predicts about the same CCD change as observed between the Panama and Guatemala basins.

The correlation between shallowing CCD and increasing productivity will only occur, however, in a region of relatively high productivity, such as the modern eastern Pacific Ocean (Archer, 1991). Here, the C_{org}:C_{CO_3} in falling sedimentary detritus is relatively high (~1), and the dissolution resulting from C_{org} degradation is accentuated. In regions having low to moderate productivity (e.g., the central equatorial Pacific Ocean and the oceanic gyres) the low C_{org}:C_{CO_3} in the particulate rain to the seafloor (~0.5) means that initial increases in productivity will deliver a larger mass of carbonate particles to surface sediments than carbonate degradation products. The carbonate MAR first will increase with productivity, and the CCD can be driven deeper. If productivity increases sufficiently, however, conditions will begin to resemble those in the eastern Pacific, and the CCD will then be driven down again.

Late Miocene Carbonate MARs and CCD Changes

Figure 9 shows maps of carbonate MARs in the eastern Pacific from 13 to 5 Ma. Data used to construct these maps are presented in Table 3. The data are averages reported at the midpoint of their range (i.e., 9 Ma data is the average of 8.75–9.25 Ma). Despite this averaging, it becomes apparent from Figure 9 that the eastern Pacific switched rapidly from an environment where carbonates were deposited relatively evenly over the entire region to a regime in which carbonate deposition was focused at the equator and little carbonate was buried in the eastern Pacific basins.

The carbonate MAR map at 13 Ma is a good illustration of the depositional environment during the late middle Miocene. Carbonate deposition was relatively uniform. Nowhere, however, was the amount of carbonate deposition high. Even Site 495, the deepest drill site in the Guatemala Basin (3800 m deep at 13 Ma), had a respectable carbonate MAR of 0.3 g/cm^2/k.y. Near equatorial sites (e.g., Site 846) had higher deposition (0.7 g/cm^2/k.y.), and gradients of carbonate MAR away from the equator were not strong. If Leg 138 and central Pacific data (van Andel et al., 1975) are examined together one can discern that the pattern of carbonate MAR at this time was shaped like a blunt wedge pointed westward. While the western Pacific equatorial carbonate zone narrowed from the late Oligocene maximum, the eastern Pacific carbonate zone remained wide. The westward extent of the equatorial carbonate zone remained stable throughout the middle Miocene (van Andel et al., 1975).

Carbonate MARs at 11 Ma foreshadow the late Miocene carbonate crash (Fig. 9). Carbonate deposition everywhere is low, even though the CCD is still relatively deep. In the Guatemala Basin, for example, the CCD was deeper than 4000 m (Fig. 10). Throughout the region, sedimentation rates were still high, but rates were beginning to decline from peaks in the middle Miocene (Fig. 11). Changes in carbonate MAR between 13 and 11 Ma seem to have been caused mostly by a slowdown in carbonate production, not by an increase in

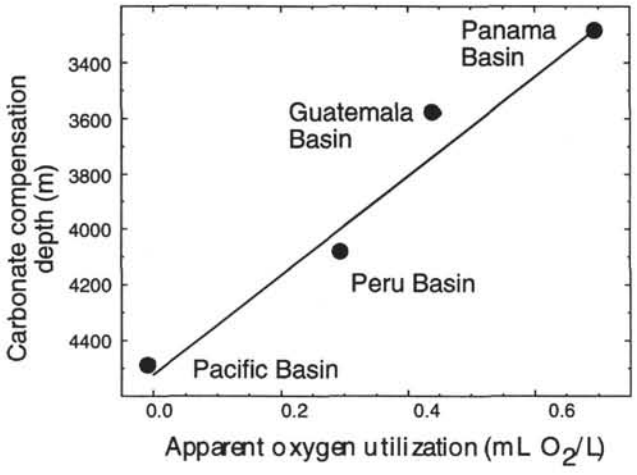

Figure 8. Relationship between apparent oxygen utilization (AOU) in each of the eastern Pacific basins and CCD. A value of 1 mL O_2/L oxygen consumption causes a rise in CCD of about 1780 m. Oxygen data for Peru, Panama, and the Pacific Basin regions can be found in Lonsdale (1976), while Guatemala Basin deep-water data are from unpublished WOCE surveys in the region.

dissolution rate (Fig. 12). Increased etching of preserved nannofossil assemblages, for example, occurs for the most part after 11 Ma (Farrell et al., this volume).

The CCD east of the EPR rose to such an extent by 10 Ma that all eastern sites were near it (Fig. 9). The CCD rose nearly to the paleodepth of Site 846, then at 3255 mbsl. Between 10 and 9 Ma, the CCD sometimes rose above Site 846 and no carbonate at all was deposited there. Sedimentation rates in the interval between 10 and 8 Ma typically are at the lowest levels approached in the Miocene throughout the eastern Pacific (Fig. 11). Farther west, carbonate deposition in the central equatorial Pacific contracted until it was limited to a narrow band along the equator (van Andel et al., 1975).

The CCD in the Guatemala Basin shallowed by about 800 m (Fig. 10) at 10 Ma, and stayed high from 10 to 0 Ma. Carbonate deposition at Site 319 in the Peru (Bauer) Basin also ends about this time, so it appears that all eastern Pacific basins were affected similarly. The carbonate lysocline in the equatorial Pacific must have risen abruptly at 10 Ma, indicated by the number of sites having carbonate MARs of less than 1 g/cm^2/k.y. (Table 3). Clearly, the carbonate crash was felt throughout the Pacific, although the strongest effects appeared east of the EPR.

Recovery from the late Miocene carbonate crash was under way by 8 Ma (Fig. 9) and followed the equatorial high productivity band. On the Leg 138 transect west of the EPR, near-equatorial drill sites again had carbonate MARs greater than 1 g/cm^2/k.y. Nevertheless, the Guatemala and Peru basins never again had high carbonate deposition except on their shallow flanks. The CCD in the Guatemala Basin appears to have hovered at a depth of about 3400 m from 10 Ma onward, deepening at some time in the Pliocene–Pleistocene to the modern CCD at 3600 mbsl (Figs. 10 and 7). Sites 503 (Guatemala Basin) and 84 (Panama Basin) may show a recovery from the carbonate crash. Because both sites are shallow and near the equator, they form part of the equatorial high carbonate band.

Between 7 and 6 Ma, carbonate MARs reached their all-time peaks throughout the eastern Pacific, with the exception of the bathyal sites east of the EPR. This peak in carbonate MARs results primarily from the high regional sedimentation rates during the latest part of the Miocene (Fig. 11), which probably resulted from high primary productivity and high carbonate production in surface waters.

DISCUSSION

At about 10 Ma, the eastern Pacific changed from a regime where carbonate MARs were controlled by relatively low dissolution to one in which variable production of carbonate competed with a strong dissolution loss in the deep parts of the sedimentary basins. We postulate that the switch in regimes was caused by the restriction of the flow of deep waters rich in $[CO_3]^{2-}$ from the Atlantic through the Panama gateway. Neither productivity nor changes in sea level would produce the observed eastern Pacific carbonate MAR patterns.

Productivity and CCD Rise in the Eastern Pacific

While it is possible that a dramatic increase in primary productivity in the eastern Pacific could have caused the carbonate crash at 10 Ma, the magnitude of such a productivity event should have left abundant evidence in the sediments. Such evidence does not exist.

Based upon the modern relationships between the CCD and productivity discussed earlier, one can roughly calculate the increase in productivity needed to cause the late Miocene carbonate crash. The CCD in the Guatemala Basin rose by 800 m at 10 Ma. A similar rise probably occurred in the Peru and Panama basins, although there are insufficient numbers of drill sites to quantify the CCD depth in either basin. To change the CCD by 800 m requires an increase by about a factor of eight in average productivity in the region east of the EPR. This level of productivity must then have been sustained from 10 Ma until the present.

An increase in productivity having a factor of eight should be readily apparent in C_{org} MARs (Müller and Suess, 1979; Sarnthein et al., 1988; Lyle et al., 1988, 1992). Export of particulate C_{org} rain from surface water and preservation increase nonlinearly with productivity increases. For this reason, a much higher fraction of total productivity is exported from highly productive surface waters than from those of lower productivity (Eppley and Peterson, 1979). An increase in productivity by a factor of eight thus should have caused a much larger increase in C_{org} rain—at least by an order of magnitude and maybe more.

Increases in preservation of sedimentary C_{org} are strongly related to C_{org} rain, which should further amplify the C_{org} MAR signal relative to the productivity change. Lyle et al. (1992), for example, observed a 30-fold increase of C_{org} MAR along the Multitracers transect in the northeastern Pacific as a result of a four-fold increase in C_{org} rain. The enhancement of C_{org} MAR relative to C_{org} rain results from the depletion of oxygen and other oxidizing agents from pore waters. The net result is that an eight-fold increase in productivity could cause an increase in C_{org} MAR by about two orders of magnitude.

In contrast, the Leg 138 Shipboard Scientific Party observed a decrease in C_{org} MAR between 12 and 9 Ma at all sites except Site 846 (Mayer, Pisias, Janecek, et al., 1992). One cannot explain the huge difference between observation and prediction by assuming that C_{org} MAR systematics are poorly understood. No processes of C_{org} degradation could suppress such a major C_{org} MAR signal. Every change needed to raise the CCD by productivity, in turn, would enhance the preservation of C_{org} in the sediments. Thus, we can confidently rule out productivity as a factor in the carbonate crash.

Sea Level and CCD Change

Sea level can also be ruled out as a major contributing factor to the carbonate crash because the decrease in sea level at 10 Ma probably deepened the CCD, rather than raised it (Berger and Winterer, 1974; Opdyke and Wilkinson, 1988; Peterson et al., 1992). The continental shelves can apparently act as a much larger reservoir for carbonates than for C_{org}. Barron (1985) assumed that loss of C_{org} from continental shelves would be more significant when he proposed that lowered sea

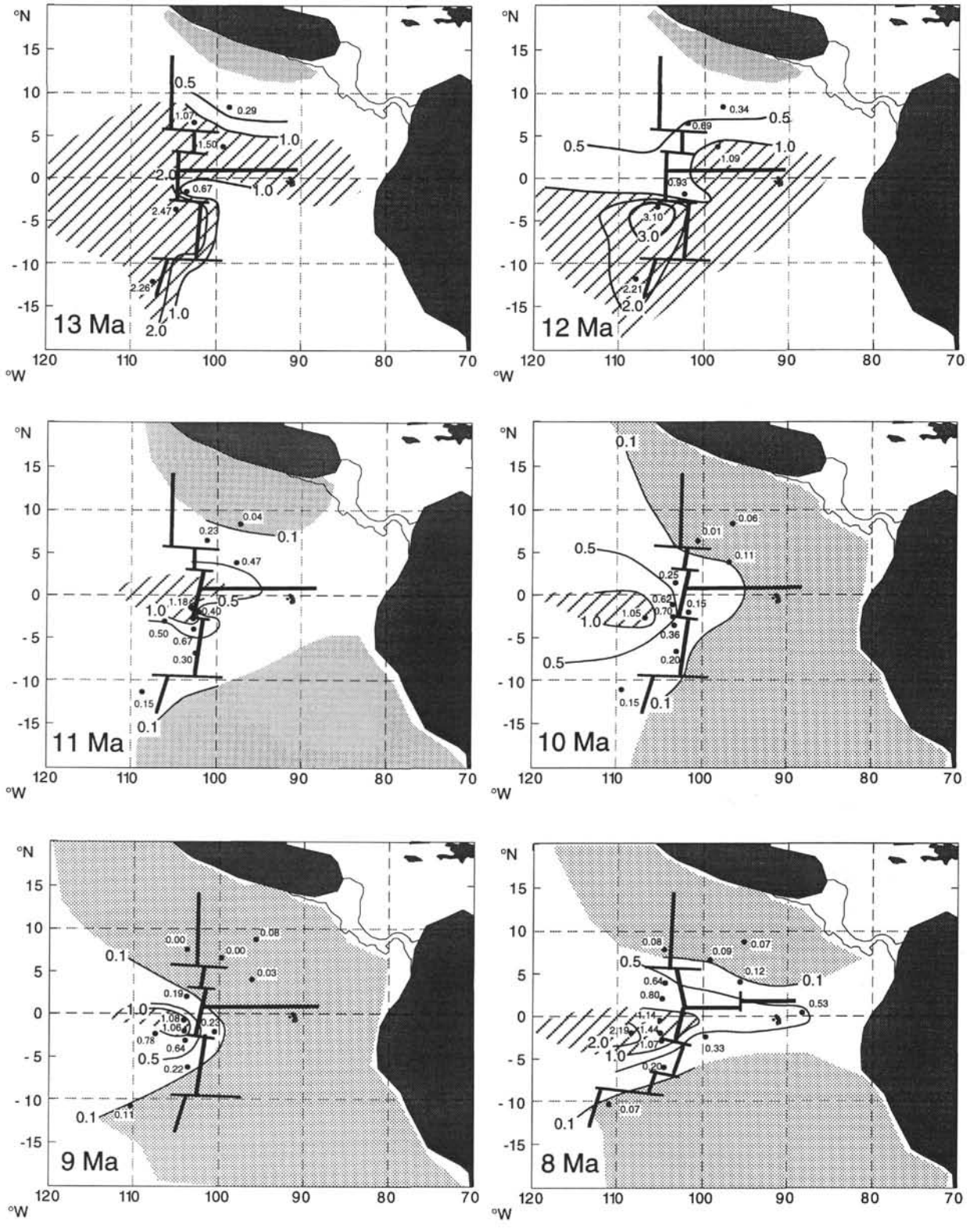

Figure 9. Maps of calcium carbonate MAR from 13 to 5 Ma. Stippled pattern marks areas below the CCD (<0.1 g/cm^2/k.y.), while striped areas mark MARs higher than 1.0 g/cm^2/k.y. Note that widespread carbonate deposition in the middle Miocene was replaced abruptly at 10 Ma by a deposition pattern much more focused at the equator. The CCD rose by at least 800 m in the Guatemala Basin in less than 0.5 m.y., and a similar rise was experienced elsewhere east of the EPR.

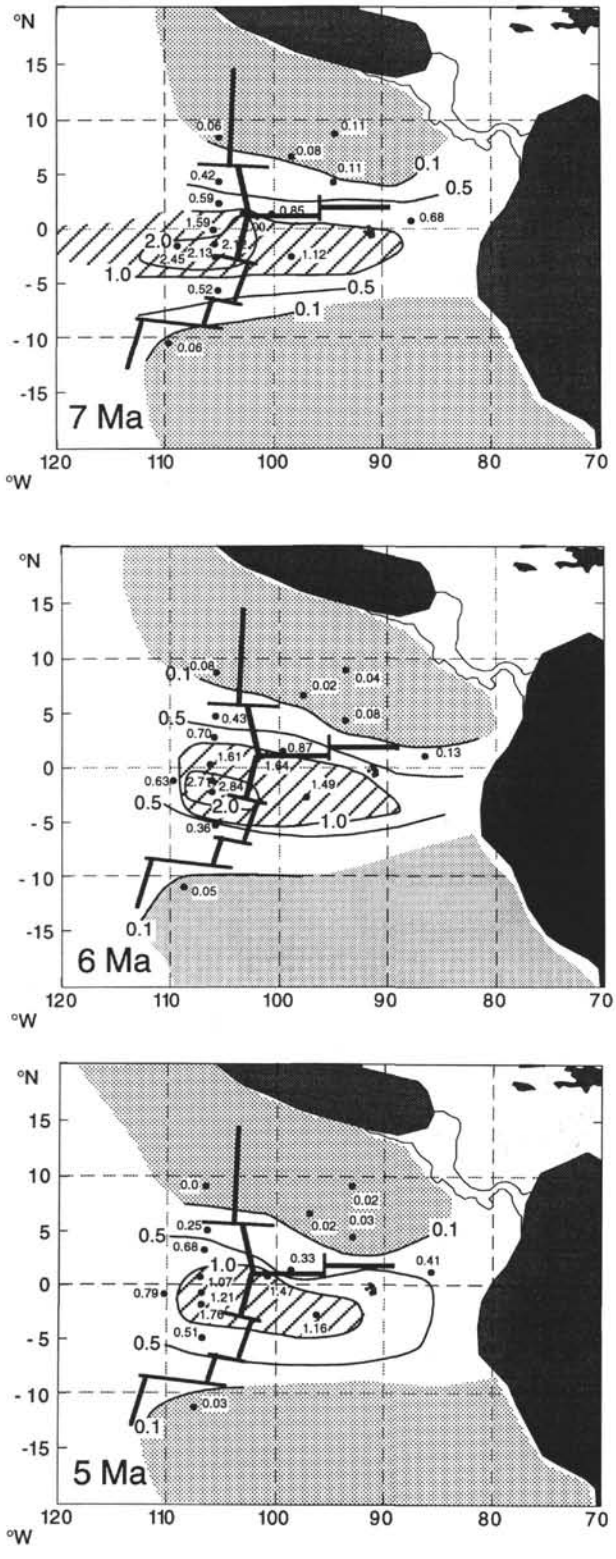

Figure 9 (continued).

level at the middle/late Miocene transition could have caused the carbonate dissolution event in the eastern Pacific. Empirical comparisons between CCD reconstructions and global sea level changes (e.g., Peterson et al., 1992), however, show that the middle/late Miocene decline in sea level is associated with a deepening of the CCD and enhanced carbonate preservation over much of the oceans.

The abrupt rise in CCD in the eastern Pacific documented here runs counter to this general trend. The probable cause of the carbonate crash, therefore, must be regional in nature. Such a regional response must have been caused by changes in deep-water circulation patterns.

Changes in Deep Water and the Carbonate Crash

The late Miocene carbonate crash marks a time when $[CO_3]^{2-}$ in deep waters of the eastern Pacific basins must have dropped radically. The rise in CCD results from dissolution of particulate carbonate to compensate for this loss. The change in deep water $[CO_3]^{2-}$ may have been caused by a variety of reorganizations in deep water flow, but the one that seems most likely to us is a constriction of the Panama Gateway and restriction of flow of relatively high $[CO_3]^{2-}$ waters from the Atlantic to the eastern Pacific.

Alternative Scenario—NADW Initiation

The crash could be associated with the onset of North Atlantic Deep Water (NADW) formation and the global reorganization of deep-water circulation at about this time (Woodruff and Savin, 1989). Initiation of NADW formation, however, should tend to make global bottom waters less corrosive to carbonates. NADW is formed from Atlantic surface waters low in nutrients and, consequently, with low total dissolved inorganic carbon (DIC) and high titration alkalinity, and thus high $[CO_3]^{2-}$. These deep waters should in part replace more corrosive deep waters formed in the Antarctic Ocean from more nutrient-rich waters and thus enhance carbonate preservation.

The response in the Pacific depends, however, upon how flow paths reorganized. If the reorganization initiated by the onset of NADW formation enhanced the import of Antarctic-origin deep waters into the Pacific, at least part of the late Miocene carbonate crash could have been caused by this factor. No strong evidence from oxygen and carbon isotope tracers exists for increased Antarctic-source waters in the Pacific Ocean at 11 to 10 Ma, but such increases are difficult to detect by isotopes. The sparse faunal evidence (Woodruff and Savin, 1989) shows increased fractionation between the South Atlantic and South Pacific deep waters at about this time, but does not really indicate stronger flow into the Pacific at this time.

Panama Gateway Restriction as the Cause of the late Miocene Crash

The strongest evidence for the participation of the Panama Gateway in the carbonate crash is its pattern. The crash most strongly affected the eastern Pacific basins—the CCD rose permanently there, in contrast with the transient response recorded elsewhere in the Pacific. Because the waters that fill these basins are of mid-depth origin (~3 km), they should be less sensitive to bottom water events than the deeper Pacific basins. Changes in deep-water circulation patterns that strongly affect the basins east of the EPR should have affected other parts of the Pacific Ocean more strongly. The lack of such a response indicates that the cause must have been localized within this region.

If the constriction of the Panama Gateway caused the carbonate crash, the effects of the uplift of the isthmus are first manifested about 7 m.y., before its rise above sea level, between 3.5 and 3 Ma (Saito, 1976; Keigwin, 1978; Marshall et al., 1982). This conclusion is in line with the carbon isotope evidence of Keigwin (1982) that Pacific and Atlantic deep waters on either side of the present Isthmus of Panama were significantly isolated from each other before 8 Ma. It also fits with Woodruff and Savin's (1989) observation that differences in carbon isotope composition between the Atlantic and Pacific oceans began near the start of the late Miocene.

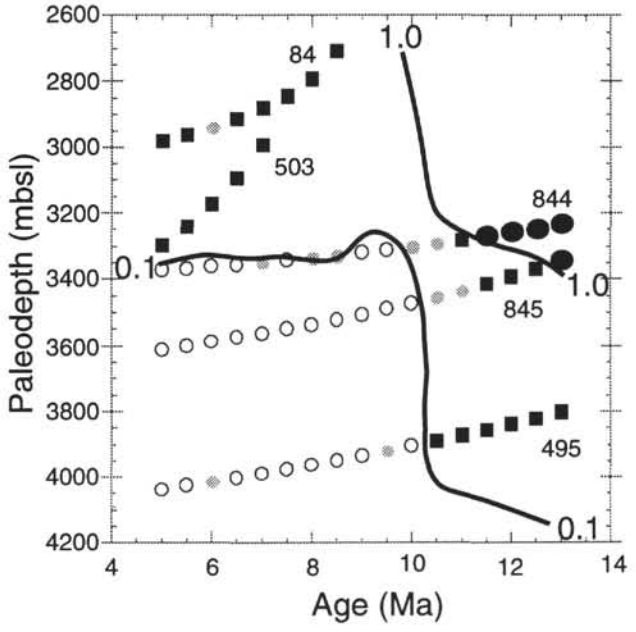

Figure 10. Changes in the Miocene CCD of the Guatemala/Panama basins. Large filled circles mark carbonate MARs in excess of 1.0 g/cm²/k.y., while large filled squares mark carbonate MARs between 0.5 and 1.0 g/cm²/k.y. Small filled circles mark carbonate MARs between 0.1 and 0.5 g/cm²/k.y., and open circles mark MARs below 0.1 g/cm²/k.y. Lines are drawn along 0.1 and 1.0 g/cm²/k.y. MAR isopleths.

Estimates of Loss of Deep-Water Flow Through the Panama Gateway

One can estimate the magnitude of change of deep-water flow from the Atlantic to the eastern Pacific, provided that the loss of carbonate MAR is entirely the result of changes in deep-water properties. Assuming that deep-water $[CO_3]^{2-}$ remained constant in the eastern Pacific, the loss of carbonate deposition throughout the region should represent the inventory of $[CO_3]^{2-}$ from the Atlantic that had to have been replaced, as follows from the budget below:

$$[CO_3]^{2-}_{EPac} = X_{Atl}\,[CO_3]^{2-}_{Atl} + X_{Pac}\,[CO_3]^{2-}_{Pac} + X_{CC}\ , \qquad (7)$$

where *EPac*, *Atl*, and *Pac* represent concentrations of $[CO_3]^{2-}$ in the eastern Pacific and Atlantic and Pacific deep-water sources. X_{Atl}, X_{Pac}, and X_{CC} represent the number of moles of water entering the basin from the Atlantic and Pacific, and the number of moles of $CaCO_3$ dissolved. By assuming a $[CO_3]^{2-}$ difference between the Atlantic and Pacific waters, one can calculate the water flow between oceans.

From Figure 9, roughly 0.5 g/cm²/k.y. of $CaCO_3$ deposition disappeared from the Guatemala Basin at 10 Ma, equivalent to a loss of 2×10^{11} mole/yr. This should represent about one-third of the net loss of $[CO_3]^{2-}$ to the eastern Pacific by constriction of the Panama Gateway, since all the other basins east of the EPR also participated.

Assuming conservatively that the difference in $[CO_3]^{2-}$ between Atlantic and Pacific deep waters was 10 µmol/kg, compared to ~30 µmol/kg today (Emerson and Archer, 1992), 0.6 Sv (10^6 m³/s) of flow into the Guatemala Basin from the Atlantic was replaced by flow from the Pacific. Thus, net flow through the Panama gateway need only have been restricted by about 2 Sv to produce the dramatic change in regional carbonate preservation east of the EPR.

Recovery from the Carbonate Crash

For most of the equatorial Pacific, the late Miocene carbonate crash ended about 8 Ma. In the eastern Pacific, the recovery appears to have been induced be a long-lived high productivity interval beginning about 8 Ma and ending at about 4.5 Ma. After 8 Ma, carbonate MARs increased within the equatorial band throughout the eastern Pacific and peaked between 6 and 7 Ma (Fig. 9). Little or no deposition occurred on the floors of the eastern Pacific basins during this time, however, because CCDs east of the EPR remained high for the remainder of the Miocene.

We think that the high equatorial carbonate MARs were caused by increased productivity because this interval is associated with a peak in sedimentation rates and a peak in C_{org} and carbonate MARs at all Leg 138 drill sites, except those in the Guatemala Basin (Fig. 11), and because the pattern of carbonate MAR is focused around the equator, reminiscent of equatorial upwelling patterns (Fig. 9).

Earlier we discussed how higher productivity could cause increased dissolution and a shallowing of the CCD. This does not contradict the conclusion advanced here because, depending on the circumstances, a productivity increase could either increase or decrease carbonate MARs. Since carbonate dissolution depends upon both the saturation state of bottom waters and the particulate C_{org}:C_{CO_3} ratio, the likelihood of increased carbonate burial depends upon its depth and the level of productivity prior to the increase. The total amount of carbonate dissolution from marine sediments is the sum of dissolution caused by the well-known depth dependent undersaturation effect and dissolution within the sediments caused by C_{org} decomposition. As the relative proportion of C_{org} to carbonate increases with increasing productivity, dissolution by C_{org} degradation becomes a significant fraction of the total carbonate loss. Within the lysocline, dissolution associated with C_{org} degradation can completely deplete the sediments of carbonate well above the CCD caused solely by pressure effects. Thus, an increase in productivity can raise the CCD. Nevertheless, in relatively shallow sediments, in the upper part of the lysocline or above it, an increase in productivity will tend to increase carbonate MARs. Between 8 to 4.5 Ma, all the Leg 138 drill sites east of EPR with high carbonate MARs are shallower than 3300 mbsl and thus represent locations which should have higher carbonate MARs when productivity increases.

CONCLUSIONS

The late Miocene carbonate crash was an abrupt rise in CCD at 10 Ma, especially pronounced in the eastern Pacific Ocean. West of the EPR, this event lasted about 2 to 3 m.y., and carbonate MARs rapidly recovered. In the Guatemala and Peru basins, however, the carbonate crash marks the end of bathyal carbonate deposition in the basins. The shallow CCDs established east of the EPR by this event are the basis of the modern pattern of carbonate MAR.

The carbonate crash was caused by deep-water processes, not by high productivity. We have documented that the observed changes in paleoproductivity that can be inferred from the sediment record could not have caused the rise in CCD. We have shown that a relatively small decrease in net exchange of deep waters from the Atlantic to the Pacific through the Panama Gateway, however, could have caused it. For this reason, we think that the carbonate crash was induced by a tectonic restriction of deep-water flow through the Panama Gateway at about 10 Ma. The tectonic restriction of flow essentially set up the modern pattern of carbonate deposition in the eastern Pacific.

Most of the equatorial Pacific Ocean recovered from the carbonate crash relatively quickly. The recovery seems associated with a long-lived high productivity event that lasted from about 8 to about 4.5 Ma. High carbonate MARs were probably more restricted to regions of high carbonate production than at earlier times, partly because the

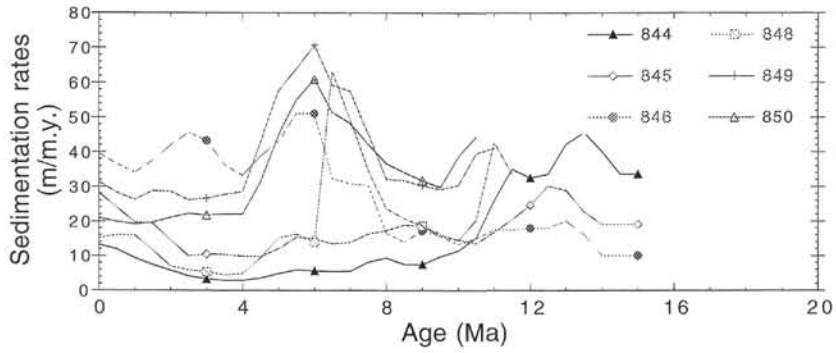

Figure 11. Sedimentation rates for Leg 138 cores that extend to 12 Ma. Note that sedimentation rates reached a major low in the late Miocene (10–9 Ma) and peaked at about 6 Ma. There is no evidence for higher productivity and higher sediment deposition at the middle/late Miocene transition.

fractionation of nutrients between the Atlantic and Pacific oceans was beginning to accelerate after communication between the two became more restricted.

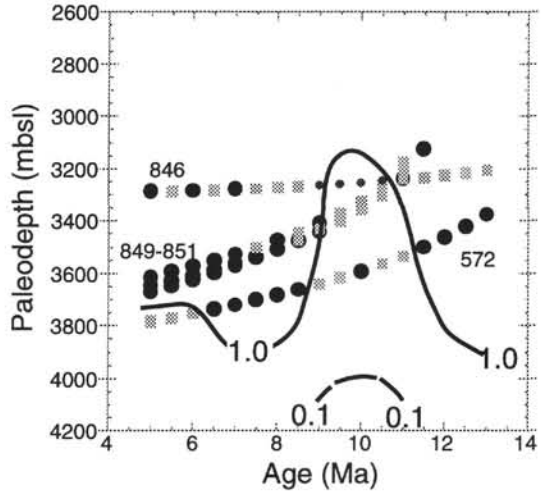

Figure 12. Changes in the Miocene CCD of the equatorial Pacific region. Large filled circles mark carbonate MARs in excess of 1.0 g/cm^2/k.y., while large filled squares mark carbonate MARs between 0.5 and 1.0 g/cm^2/k.y.. Small filled circles mark Carbonate MARs between 0.1 and 0.5 g/cm^2/k.y., and open circles mark MARs below 0.1 g/cm^2/k.y. Lines are drawn along 0.1 and 1.0 g/cm^2/k.y. MAR isopleths. Site 846, east of the EPR crest, consistently has lower carbonate deposition than drill sites to the west, despite having the highest Pliocene–Pleistocene sedimentation rates.

REFERENCES*

Archer, D., 1991. Modeling the calcite lysocline. *J. Geophys. Res.*, 96:17037–17050.

Barron, J.A., 1985. Diatom paleoceanography and paleoclimatology of the central and eastern Equatorial Pacific between 18 and 6.2 Ma. *In* Mayer, L., Theyer, F., Thomas, E., et al., *Init. Repts. DSDP*, 85: Washington (U.S. Govt. Printing Office) 935–945.

Berger, W.H., and Winterer, E.L., 1974. Plate stratigraphy and the fluctuating carbonate line. *In* Hsü, K.J., and Jenkyns, H.C. (Eds.), *Pelagic Sediments on Land and Under the Sea.* Spec. Publ. Int. Assoc. Sedimentol., 1:11–48.

Demets, C., Gordon, R.G., Argus, D.F., and Stein, S., 1990. Current plate motions. *Geophys. J. Int.*, 101:425–478.

Dymond, J., Corliss, J.B., and Heath, G.R., 1977. History of metalliferous sedimentation at Deep Sea Drilling Project site 319, in the South eastern Pacific. *Geochim. Cosmochim. Acta*, 41:741–753.

Dymond, J., and Lyle, M., 1985. Flux comparisons between sediments and sediment traps in the eastern tropical Pacific: implications for atmospheric CO_2 variations during the Pleistocene. *Limnol. Oceanogr.*, 30:699–712.

Emerson, S., and Archer, D., 1992. Glacial carbonate dissolution cycles and atmospheric pCO_2: a view from the ocean bottom. *Paleoceanography*, 7:319–331.

Emerson, S., and Bender, M., 1981. Carbon fluxes at the sediment-water interface of the deep-sea: calcium carbonate preservation. *J. Mar. Res.*, 39:139–162.

Engebretson, D.C., Cox, A., and Gordon, R.G., 1985. *Relative Motions Between Oceanic and Continental Plates in the Pacific Basin.* Spec. Pap.—Geol. Soc. Am., 206.

Eppley, R.W., and Peterson, B.J., 1979. Particulate organic matter flux and planktonic new production in the deep ocean. *Nature*, 282:677–680.

Farrell, J.W., and Prell, W.L., 1989. Climatic change and $CaCO_3$ preservation: an 800,000 year bathymetric reconstruction from the central equatorial Pacific Ocean. *Paleoceanography*, 4:447–466.

Finney, B.P., Lyle, M.W., and Heath, G.R., 1988. Sedimentation at MANOP Site H (eastern equatorial Pacific) over the past 400,000 years: climatically induced redox variations and their effects on transition metal cycling. *Paleoceanography*, 3:169–189.

Hamilton, E.D., 1976. Variations of density and porosity with depth in deep-sea sediments. *J. Sediment. Petrol.*, 46:280–300.

Karlin, R., Lyle, M., and Zahn, R., 1992. Carbonate variations in the Northeast Pacific during the late Quaternary. *Paleoceanography*, 7:43–61.

Keigwin, L.D., Jr., 1978. Pliocene closing of the Isthmus of Panama, based on biostratigraphic evidence from nearby Pacific Ocean and Caribbean Sea cores. *Geology*, 6:630–634.

———, 1982. Stable isotope stratigraphy and paleoceanography of Sites 502 and 503. *In* Prell, W.L., Gardner, J.V., et al., *Init. Repts. DSDP*, 68: Washington (U.S. Govt. Printing Office), 445–453.

Keller, G., and Barron, J.A., 1983. Paleoceanographic implications of Miocene deep-sea hiatuses. *Geol. Soc. Am. Bull.*, 94:590–613.

Koblenz-Mishke, O.I., 1965. The value of primary production in the Pacific Ocean. *Okeanol. Moscow*, 4:458–461.

Lonsdale, P., 1976. Abyssal circulation of the southeastern Pacific and some geological implications. *J. Geophys. Res.*, 81:1163–1176.

Love, C.M. (Ed.), 1972. *EASTROPAC Atlas 6.* Dept. of Commerce Circ., 330.

Love, C.M., and Allen, R.M. (Eds.), 1975. *EASTROPAC Atlas 10*: Dept. of Commerce Circ., 330.

Lyle, M., 1992. Composition maps of surface sediments of the eastern tropical Pacific Ocean. *In* Mayer, L., Pisias, N., Janecek, T., et al., *Proc. ODP, Init. Repts.*, 138 (Pt. 1): College Station, TX (Ocean Drilling Program), 101–115.

Lyle, M., Murray, D.W., Finney, B.P., Dymond, J., Robbins, J.M., and Brooksforce, K., 1988. The record of late Pleistocene biogenic sedimentation in the eastern tropical Pacific Ocean. *Paleoceanography*, 3:39–59.

Lyle, M., Zahn, R., Prahl, F., Dymond, J., Collier, R., Pisias, N., and Suess, E., 1992. Paleoproductivity and carbon burial across the California Current: the Multitracers Transect, 42°N. *Paleoceanography*, 7:251–272.

Mammerickx, J., and Klitgord, K.D., 1982. Northern East Pacific Rise: evolution from 25 m.y. B.P. to the present. *J. Geophys. Res.*, 87:6751–6759.

*Abbreviations for names of organizations and publications in ODP reference lists follow the style given in *Chemical Abstracts Service Source Index* (published by American Chemical Society).

Mammerickx, J., and Naur, D.F., 1988. The Mathematician paleoplate. *J. Geophys. Res.*, 93:3025–3040.

Marshall, L.G., Webb, S.D., Sepkoski, J.J., Jr., and Raup, D.M., 1982. Mammalian evolution and the great American interchange. *Science*, 215:1351–1357.

Mayer, L.A., 1991. Extraction of high-resolution carbonate data for paleoclimate reconstruction. *Nature*, 352:148–150.

Mayer, L.A., Pisias, N.G., Janecek, T.R., et al., 1992. *Proc. ODP, Init. Repts.* 138 (Pts. 1 and 2): College Station, TX (Ocean Drilling Program).

Mayer, L.A., Shipley, T.H., and Winterer, E.L., 1986. Equatorial Pacific seismic reflectors as indicators of global oceanographic events. *Science*, 233:761–764.

Müller, P.J., and Suess, E., 1979. Productivity, sedimentation rate, and sedimentary organic matter in the oceans. I. Organic carbon preservation. *Deep-Sea Res. Part A*, 26:1347–1362.

Opdyke, B.N., and Wilkinson, B.H., 1988. Surface area control of shallow cratonic to deep marine carbonate accumulation. *Paleoceanography*, 3:685–703.

Peterson, L.C., Murray, D.W., Ehrmann,W.U., and Hempel, P., 1992. Cenozoic carbonate accumulation and compensation depth changes in the Indian Ocean. *In* Duncan, R.A., Rea, D.K., Kidd, R.B., von Rad, U.,and Weissel, J.K. (Eds.), *Synthesis of Results from Scientific Drilling in the Indian Ocean.* Am. Geophys Union, Geophys. Monogr., 70:311–333.

Saito, T., 1976. Geologic significance of coiling direction in the planktonic foraminifer *Pulleniatina. Geology*, 4:305–309.

Sarnthein, M., Winn, K., Duplessy, J.-C., and Fontugne, M.R., 1988. Global variations of surface ocean productivity in low and mid latitudes: influence on CO_2 reservoirs of the deep ocean and atmosphere during the last 21,000 years. *Paleoceanography*, 3:361–399.

Theyer, F., Mayer, L.A., Barron, J.A., and Thomas, E., 1985. The equatorial Pacific high-productivity belt: elements for a synthesis of Deep Sea Drilling Project Leg 85 results. *In* Mayer, L., Theyer, F., Thomas, E., et al., *Init. Repts. DSDP*, 85: Washington (U.S. Govt. Printing Office), 971–985.

van Andel, T.H., Heath, G.R., and Moore, T.C., Jr., 1975. Cenozoic history and paleoceanography of the central equatorial Pacific Ocean. *Mem.—Geol. Soc. Am.*, 143.

Weliky, K., Suess, E., Ungerer, C.A., Müller, P.J., and Fischer, K., 1983. Problems with accurate carbon measurements in marine sediments: a new approach. *Limnol. Oceanogr.*, 28:1252–1259.

Wilson, D.S., 1993. Relative motions of the Cocos, Nazca, and Pacific plates. *Eos*, 74:585.

Woodruff, F., and Savin, S.M., 1989. Miocene deepwater oceanography. *Paleoceanography*, 4:87–140.

Date of initial receipt: 29 March 1993
Date of acceptance: 17 May 1994
Ms 138SR-157